

ARTICLE



EZH2 PROTACs target EZH2- and FOXM1-associated oncogenic nodes, suppressing breast cancer cell growth

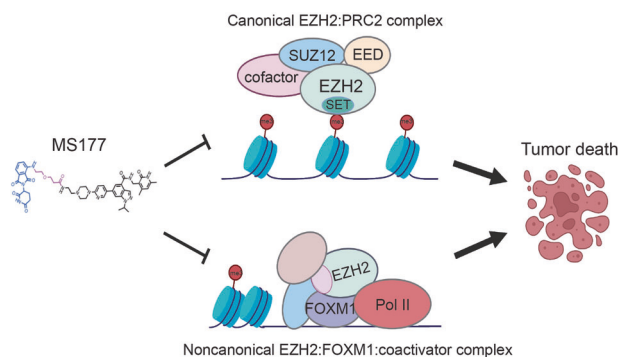
Joshua Corbin^{1,2}, Xufen Yu^{3,4}, Jian Jin^{3,4}, Ling Cai^{2,5,6}✉ and Gang Greg Wang^{1,2,5,6}✉

© The Author(s), under exclusive licence to Springer Nature Limited 2024

Breast cancer (BC) remains the second leading cause of cancer-related mortalities in women. Resistance to hormone therapies such as tamoxifen, an estrogen receptor (ER) inhibitor, is a major hurdle in the treatment of BC. Enhancer of zeste homolog 2 (EZH2), the methyltransferase component of the Polycomb repressive complex 2 (PRC2), has been implicated in tamoxifen resistance. Evidence suggests that EZH2 often functions noncanonically, in a methyltransferase-independent manner, as a transcription coactivator through interacting with oncogenic transcription factors. Unlike methyltransferase inhibitors, proteolysis targeting chimeras (PROTAC) can suppress both activating and repressive functions of EZH2. Here, we find that EZH2 PROTACs, MS177 and MS8815, effectively inhibited the growth of BC cells, including those with acquired tamoxifen resistance, to a much greater degree when compared to methyltransferase inhibitors. Mechanistically, EZH2 associates with forkhead box M1 (FOXM1) and binds to the promoters of FOXM1 target genes. EZH2 PROTACs induce degradation of both EZH2 and FOXM1, leading to reduced expression of target genes involved in cell cycle progression and tamoxifen resistance. Together, this study supports that EZH2-targeted PROTACs represent a promising avenue of research for the future treatment of BC, including in the setting of tamoxifen resistance.

Oncogene; <https://doi.org/10.1038/s41388-024-03119-9>

Graphical Abstract



INTRODUCTION

Breast cancer (BC) is the most commonly diagnosed and second leading cause of cancer-related deaths in women in the USA [1]. The expression of three proteins, estrogen receptor (ER), progesterone receptor (PR) and human epidermal growth factor receptor 2 (HER2), is used to stratify BC cases into four different molecular subtypes: Luminal A (LumA, ER + /PR + /HER2-), Luminal B (LumB, Hormone receptor + (ER and/or PR)/HER2 +), HER2-enriched (often ER-/PR- and HER2 +), and triple negative (or basal) breast cancer (TNBC, ER-/PR-/HER2-) [2, 3]. TNBC diagnosis is

associated with poorer prognosis when compared to the other molecular subtypes, largely due to a lack successful therapeutic strategies [4]; however, hormone receptor-positive BC is more common, with LumA accounting for roughly 60–65% of BC diagnoses [5]. Local LumA BC typically responds better to hormone therapies, such as the direct ER inhibitor tamoxifen (87% 25-year disease-free survival rate for LumA vs 67% for LumB for patients diagnosed without lymph node involvement) [6]; however, patients diagnosed with metastatic disease have a worse prognosis for both subtypes [7]. Due to the commonality and the

¹Department of Pharmacology and Cancer Biology, Duke University School of Medicine, Durham, NC 27710, USA. ²Duke Cancer Institute, Duke University School of Medicine, Durham, NC 27710, USA. ³Departments of Pharmacological Sciences and Oncological Sciences, Tisch Cancer Institute, Icahn School of Medicine at Mount Sinai, New York, NY 10029, USA. ⁴Mount Sinai Center for Therapeutics Discovery, Icahn School of Medicine at Mount Sinai, New York, NY 10029, USA. ⁵Department of Pathology, Duke University School of Medicine, Durham, NC 27710, USA. ⁶Department of Biochemistry and Biophysics, University of North Carolina at Chapel Hill School of Medicine, Chapel Hill, NC 27599, USA. ✉email: ling.cai@duke.edu; greg.wang@duke.edu

Received: 19 June 2024 Revised: 24 July 2024 Accepted: 29 July 2024

Published online: 07 August 2024

problem of hormone therapy resistance, work remains to improve upon the current management of LumA BC.

The enhancer of zeste homolog 2 (EZH2) is the catalytic methyltransferase member of the polycomb repressive complex 2 (PRC2) [8, 9]. EZH2 in complex with other core PRC2 members,

including embryonic ectoderm development (EED) and Suppressor Of Zeste 12 (SUZ12), catalyzes the trimethylation of histone 3 at lysine 27 (H3K27me3) – in a SET domain-dependent manner—to repress the transcription of target genes [9–11]. Through this methyltransferase-dependent canonical activity, EZH2 has been

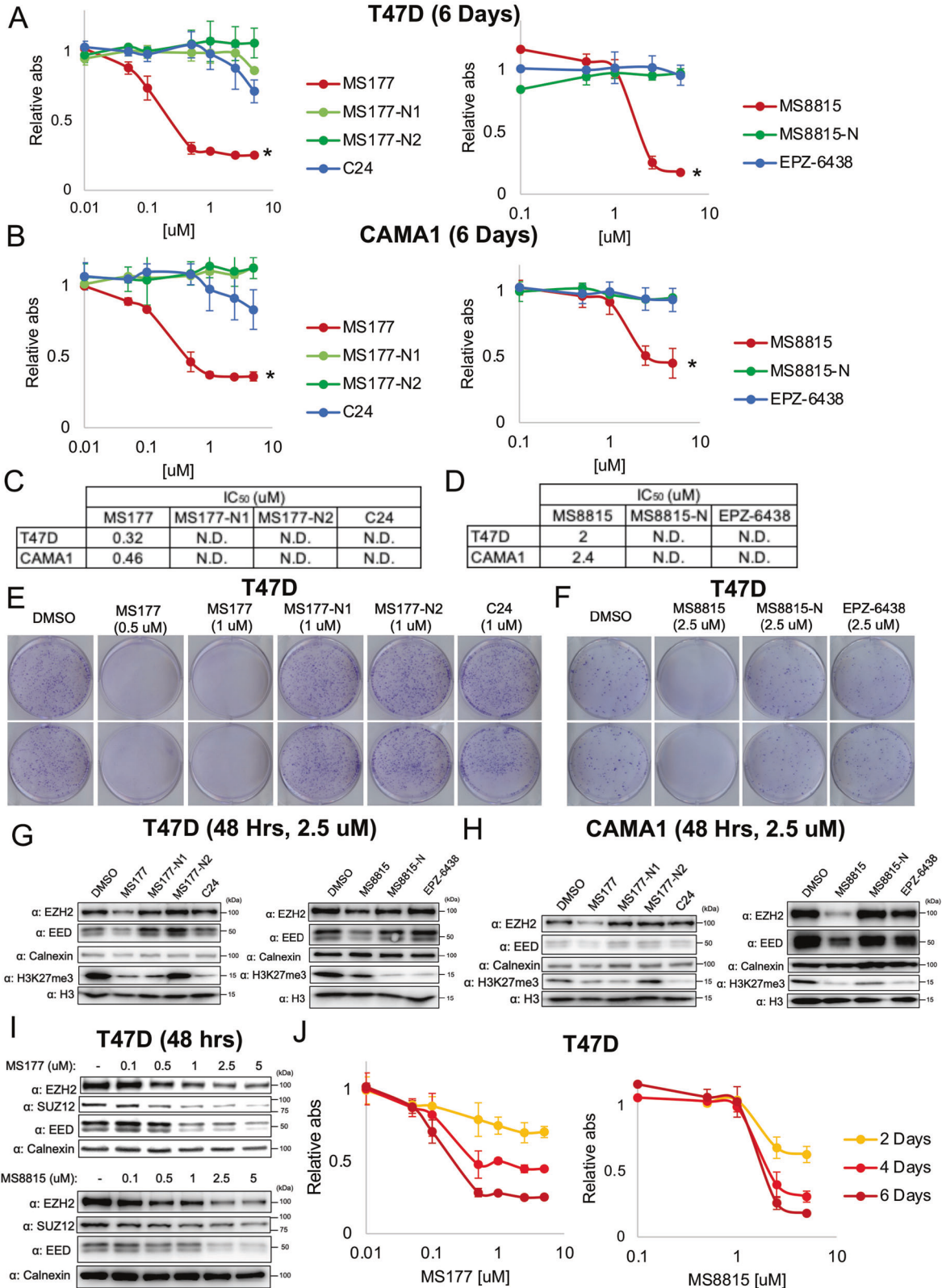


Fig. 1 MS177 and MS8815 inhibit luminal breast cancer (BC) cell growth. Plots showing relative absorbances from MTS assays of T47D (A) and CAMA1 (B) cell lines treated with labeled concentrations of MS177, controls (MS177-N1, MS177-N2), C24 (Left) or MS8815, MS8815-N, EPZ-6438 (Right). Relative absorbance numbers presented were calculated relative to cells grown treated with DMSO vehicle control. MTS assays were carried out six days after treatment of labeled compounds. $N = 3$ biological replicates. $*P < 0.05$ comparing EZH2 PROTAC to all other treatments as determined by two-sided t test and Bonferroni's adjustment. Error bars represent mean \pm s.d. Tables showing the IC_{50} growth values for MS177, MS177-N1, MS177-N2, C24 (C) and MS8815, MS8815-N, EPZ-6438 (D) in T47D and CAMA1 cell lines after six days of treatment. N.D. = Not Determined, i.e. greater than $5 \mu\text{M}$. Colony formation assays with T47D cells treated with MS177 ($0.5 \mu\text{M}$ and $1 \mu\text{M}$), $1 \mu\text{M}$ MS177-N1, MS177-N2, C24 or DMSO vehicle control (E) or $2.5 \mu\text{M}$ MS8815, MS8815-N, EPZ-6438 or DMSO vehicle control (F). Western blots showing EZH2, EED and H3K27me3 protein expression in lysates from T47D (G) and CAMA1 (H) cells treated with $2.5 \mu\text{M}$ MS177, MS177-N1, MS177-N2, C24 or DMSO vehicle control (Left) or $2.5 \mu\text{M}$ MS8815, MS8815-N, EPZ-6438 or DMSO vehicle control (Right). Cells were treated with labeled compounds for 48 h prior to cell lysis and subsequent western blot analyses. Calnexin and H3 were used as loading controls for whole cell protein and histones, respectively. The western blots were repeated for at least 2–3 times with the representative results shown here. I Western blots showing EZH2, EED and SUZ12 protein expression in lysates from T47D cells treated with labeled concentrations of MS177 (Top) or MS8815 (Bottom) or DMSO vehicle control for 48 h prior to cell lysis and subsequent western blot analyses. Calnexin was used as a loading control. The western blots were repeated for at least 2–3 times with the representative results shown here. J Plots showing relative absorbances from MTS assays of T47D cells treated with labeled concentrations of MS177 (Left) or MS8815 (Right) for 2, 4 or 6 days. Relative absorbance numbers presented were calculated relative to cells grown treated with DMSO vehicle control. $N = 3$ biological replicates. Error bars represent mean \pm s.d.

shown to repress the expression of certain tumor suppressors, including CDKN1A, and genes involved in tumor immune response [12, 13]. In BC, it has been reported that EZH2 can promote tamoxifen resistance by repressing the expression of GREB1, resulting in a redistribution of ER coregulators and ER activation in the presence of tamoxifen [14]. However, EZH2 has noncanonical gene activating functions in addition to its canonical role as a transcriptional repressor [15]. In fact, while EZH2 overexpression is associated with aggressive disease in many cancer types, including breast and prostate cancers [16, 17], studies have found that low H3K27me3 levels with high EZH2 expression is associated with worse prognosis in luminal BC [18, 19]. EZH2 has been shown to function as a coactivator of a variety of transcription factors in a methyltransferase-independent manner [20–24]. Specifically, EZH2 has been shown to function as a coactivator of hormone receptors, ER and androgen receptor (AR) [20, 23, 25], as well as, cell cycle transcription factors, such as E2F1 and MYC [22, 26]. In TNBC, hypoxia was found to induce a PRC2-independent interaction between forkhead box M1 (FOXM1) and EZH2, resulting in upregulation of the transcription of both genes and matrix metalloproteinases [27]. In luminal BC, high FOXM1 expression is associated with therapy resistance and worse prognosis [28]. These noncanonical coactivator functions of EZH2 could partly explain the lack of clinical success of EZH2 methyltransferase inhibitors in the treatment of different cancers [15, 29].

EZH2 degraders, including proteolysis targeting chimeras (PROTAC), represent one strategy through which both the canonical and noncanonical activities of EZH2 can be targeted [22, 23]. Our lab has previously shown that EZH2-targeted PROTACs, such as MS177, can be leveraged to inhibit the canonical and noncanonical activities of EZH2 by targeting EZH2 and interacting proteins for ubiquitin-mediated degradation [22, 23]. The EZH2-targeted degrader, MS1943, as well as PROTACs, U3i, MS8815 and MS177, have been reported to have antiproliferative and antitumor activities [30–32]. We hypothesize that EZH2-targeted PROTACs such as MS8815 and MS177 can be leveraged to inhibit the growth of luminal BC cells by targeting EZH2 and interacting proteins. Here, we present data suggesting that EZH2-targeted PROTACs, but not methyltransferase inhibitors, effectively inhibit luminal BC and TNBC cell growth, reduce the protein expression of the EZH2-interacting transcription factor, FOXM1, and reduce the expression FOXM1 target genes. Furthermore, these phenomena appear to be independent of ER expression and hold true in tamoxifen-resistant BC cells. Therefore, these data lay the groundwork for future studies to test the efficacy of EZH2 PROTACs in the treatment of luminal BC, including in the setting of tamoxifen resistance.

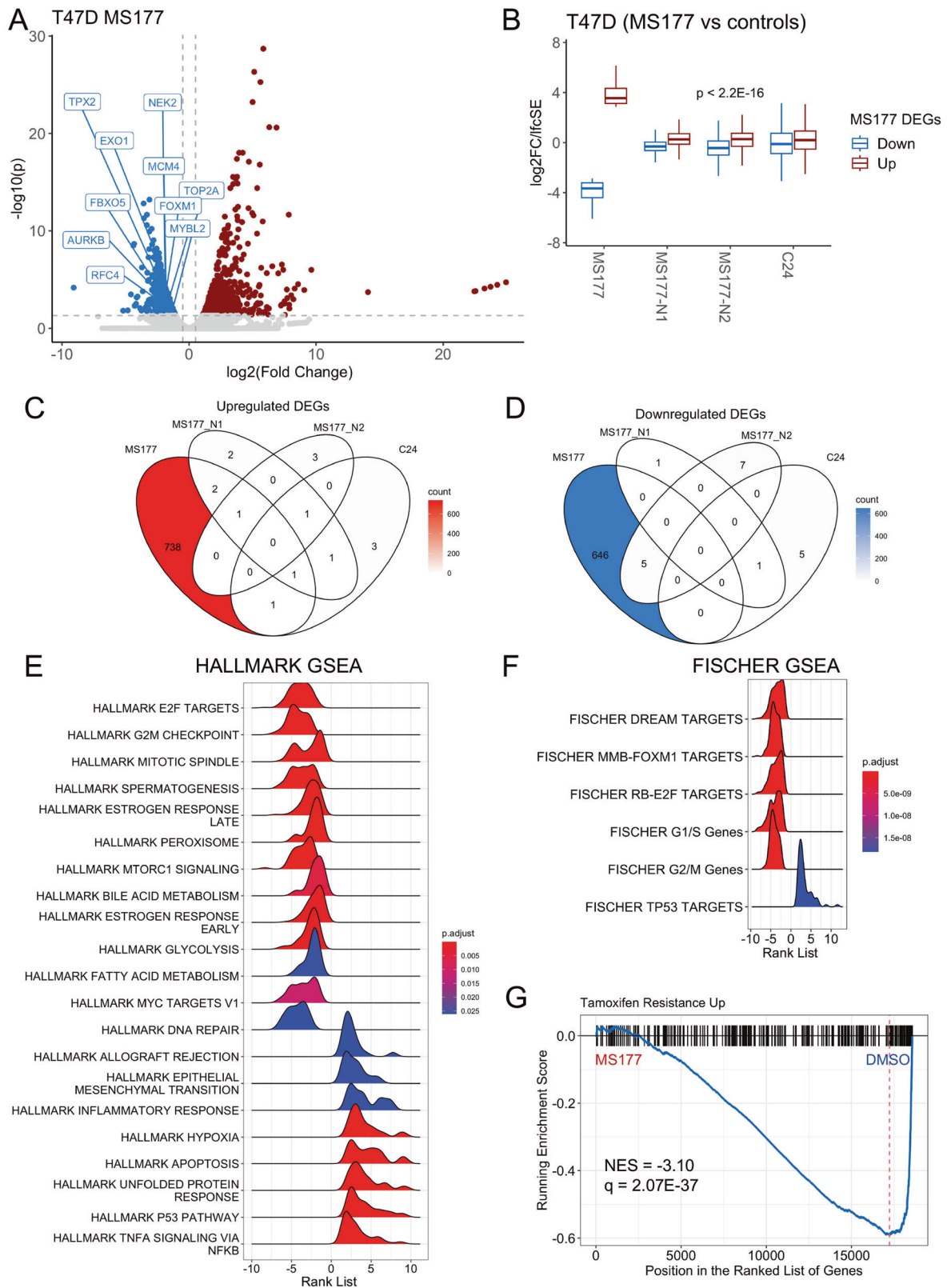
RESULTS

MS177 and MS8815 inhibit luminal breast cancer (BC) cell growth

EZH2-targeted degraders have shown promising efficacy in inhibiting the growth of TNBC cell lines [30–32]; however, it has not been tested whether EZH2-targeted PROTACs can be leveraged as growth inhibitors in luminal BC. To test this possibility, we treated luminal BC cell lines, T47D and CAMA1, with increasing doses of two EZH2-targeted PROTACs, MS177 and MS8815, in addition to negative controls (MS177-N1, MS177-N2, MS8815-N, see Fig. S1A for description of PROTACs and negative controls) and two EZH2 methyltransferase inhibitors used in PROTAC construction, C24 (used in MS177) and EPZ-6438 (used in MS8815). Both MS177 and MS8815 inhibited the growth and colony formation of these BC cells to a much larger degree when compared to their respective negative controls or matched EZH2 methyltransferase inhibitors (Fig. 1A–F); for example, IC_{50} values of MS177 were over one magnitude lower in both T47D and CAMA1 cells compared to those of C24, MS177-N1 and MS177-N2. Additionally, treatment of MS177 and MS8815 resulted in reduced protein levels of EZH2 and EED (a core PRC2 member), while both PROTACs, as well as, both methyltransferase inhibitors (C24 and EPZ-6438) and MS177-N1 and MS8815-N (which contain C24 and EPZ-6438, respectively) resulted in reductions in H3K27me3 levels in both T47D and CAMA1 cells (Fig. 1G,H). Furthermore, both MS8815 and MS177 treatment resulted in dose-dependent reductions in PRC2 protein components (EZH2, SUZ12 and EED) (Fig. 1I), as well as dose-dependent and time-dependent cell growth inhibition (Fig. 1J and S1B). Together, these results suggest that EZH2-targeted PROTACs, MS177 and MS8815, can inhibit luminal BC cell growth to a greater degree compared to their corresponding EZH2 methyltransferase inhibitors; therefore, PROTAC-mediated growth inhibition is unlikely to be due to solely inhibiting the canonical methyltransferase activity of EZH2, similar to previous studies of other cancer types in our lab and others [22, 23].

MS177 reduces the expression of cell cycle regulated and tamoxifen resistance associated genes

In order to elucidate the gene expression changes induced by EZH2-targeted PROTAC treatment, we conducted RNA-seq with RNA from T47D cells treated with $2.5 \mu\text{M}$ MS177, negative controls (MS177-N1 and MS177-N2), C24 or DMSO vehicle control for 48 h. Importantly, the growth inhibitory effects of MS177 are modest after 48 h of treatment (Fig. 1J); therefore, gene expression changes detected are less likely to be simply indirect effects of growth inhibition. MS177 treatment resulted in 743 upregulated and 651 downregulated differentially expressed genes (DEGs)



compared to DMSO control ($\log_2FC > 1$, $p_{adj} < 0.05$), many of which were cell cycle related genes (Fig. 2A). As a whole, both genes upregulated and downregulated by MS177 treatment demonstrated on average significantly less gene expression change from treatment with the other compounds (MS177-N1,

MS177-N2 or C24) (Fig. 2B; complete list in Supplemental Table 1); moreover, treatment with the other aforementioned control compounds resulted in fewer than 20 DEGs each (Fig. 2C,D). These data show that MS177 treatment uniquely results in a large number of gene expression changes compared to treatment with

Fig. 2 MS177 reduces the expression of cell cycle regulated and tamoxifen resistance associated genes. **A** Volcano plot showing log₂ fold change and $-\log_{10}$ adjusted *p* value for gene expression changes determined by RNA-seq of RNA extracted from T47D cells treated with 2.5 μ M MS177 for 48 h compared to DMSO vehicle control. Significantly upregulated and downregulated genes ($|\log_2$ fold change > 1 , adjusted *p* value < 0.05) are represented by red and blue dots, respectively. Specific example downregulated genes involved in cell cycle are labeled. **B** Box plot showing the log₂ fold change divided by standard error (log₂FC/lfcSE) values of genes significantly downregulated (blue) and upregulated (red) by MS177 determined by RNA-seq of RNA extracted from T47D cells treated with 2.5 μ M MS177, MS177-N1, MS177-N2, C24 for 48 h compared to DMSO vehicle control. *P* values were calculated comparing MS177-N1, MS177-N2 and C24 to MS177 for downregulated and upregulated genes separately using two-sided *t* test. *P* values were adjusted using Bonferroni's method, and $p < 2.2E-16$ applies to all comparisons. Venn diagrams showing genes significantly upregulated (**C**) and downregulated (**D**) by MS177, MS177-N1, MS177-N2 and C24 compared to DMSO vehicle control. Ridge plots showing HALLMARK genesets (MSigDB [54]) (**E**), Fischer cell cycle genesets [33] (**F**), with significant negative and positive associations - and enrichment plot showing tamoxifen resistance up gene set [34] (**G**) - with MS177 treatment compared to DMSO control, as determined by GSEAs from RNA-seq results. *P* values were adjusted using FDR, and *q*-values < 0.05 were considered significant.

the C24 EZH2 methyltransferase inhibitor or negative controls; mirroring the effects on cell growth (see Fig. 1).

Next, gene set enrichment analysis (GSEA) was utilized to identify gene sets and pathways affected by MS177 treatment. 21 out of 50 HALLMARK gene sets were significantly associated with MS177 treatment; in particular, cell cycle related gene sets, such as those of E2F targets, G2M checkpoint and mitotic spindle, were significantly negatively associated (downregulated) with MS177, while p53, NFKB signaling and unfolded protein response were positively associated (upregulated) with MS177 (Fig. 2E). Because cell cycle related gene sets were affected, we next conducted GSEAs with gene sets of direct targets of specific transcription factors - identified in meta-analyses by Fischer et al. [33] - that play vital roles in cell cycle progression. Both E2F and FOXM1 target gene sets, which regulate G1/S and G2/M cell cycle transitions respectively, were significantly negatively associated with MS177 treatment (Fig. 2F). Importantly, genes clinically associated with resistance to tamoxifen, many of which were shown to be related to cell cycle progression [34], were also significantly negatively associated with MS177 treatment in T47D cells (Fig. 2G). These data show that MS177 treatment reduces the expression of genes regulated during the cell cycle, in particular E2F and FOXM1 targets, as well as genes associated with tamoxifen resistance, in T47D cells. These gene expression changes were unique to MS177 treatment (compared to C24 and negative controls), correlating with the growth inhibitory effects of EZH2-targeted PROTACs (see Fig. 1).

MS177 and MS8815 inhibit growth and reduce cell cycle regulated gene sets in tamoxifen-resistant BC cells

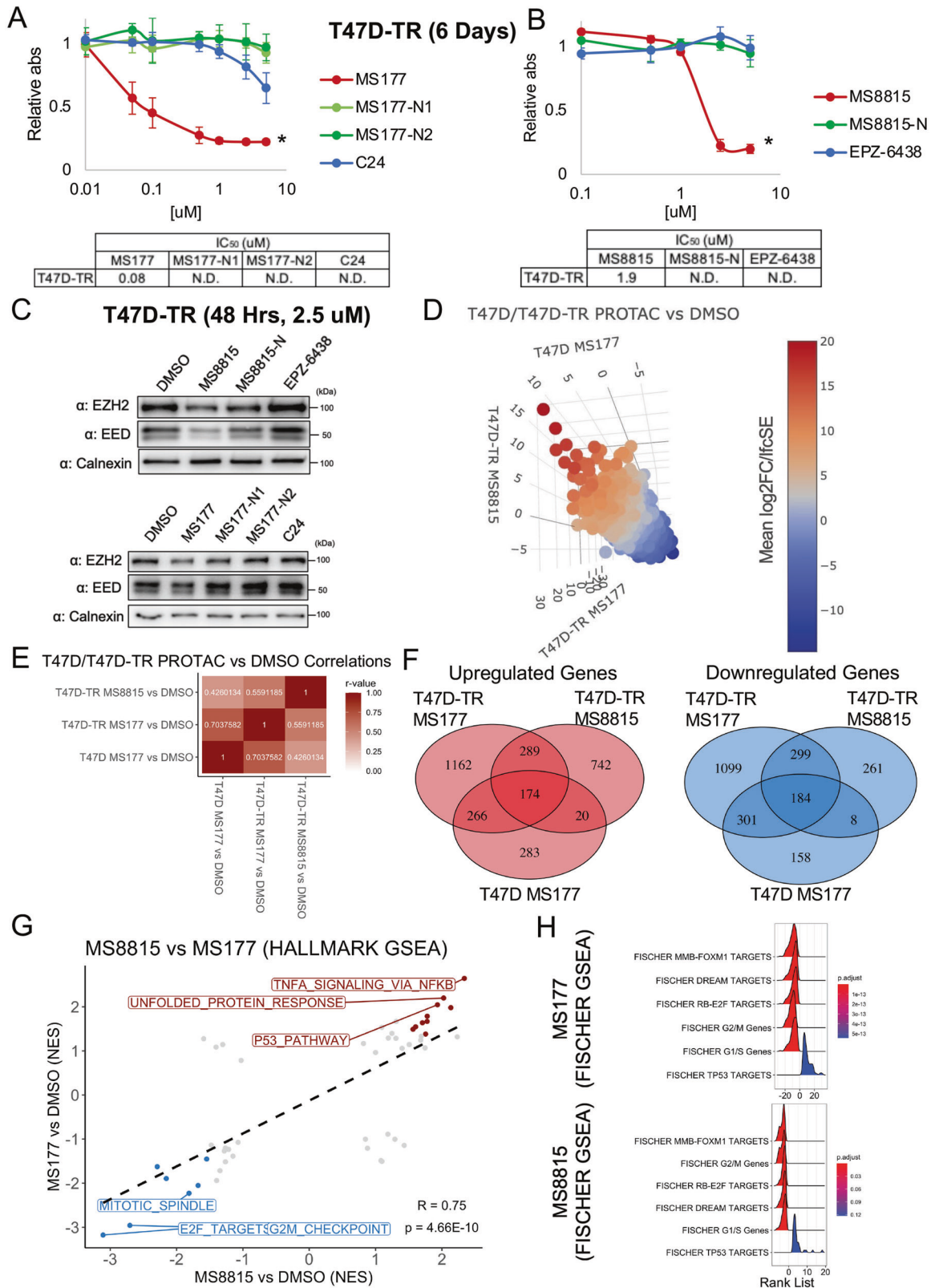
Because MS177 treatment reduced the expression of genes associated with tamoxifen resistance in T47D cells, we sought to determine whether EZH2-targeted PROTACs can also inhibit the growth of a T47D-derived cell line selected for acquired tamoxifen resistance (namely, T47D-TR). Firstly, treatment with 1 μ M tamoxifen reduced T47D-TR colony formation to a lesser degree when compared to the T47D parental cells (Fig. S2A, B), verifying the expected T47D-TR cell resistance to tamoxifen. Similar to T47D cells, MS177 and MS8815 treatment reduced the growth of T47D-TR cells in a dose-dependent manner (Fig. S2C, D), and reduced growth to a much larger degree compared to the corresponding methyltransferase inhibitors, C24 and EPZ-6438, and negative controls (Fig. 3A, B). The ability for MS177 and MS8815 to reduce EZH2 and EED protein levels in T47D-TR cells was also verified by western blot (Fig. 3C).

Next, we sought to determine the gene expression changes induced by MS177 and MS8815 treatment in T47D-TR cells. To accomplish this, RNA-seq analysis was carried out on RNA extracted from T47D-TR cells treated with: (1) 2.5 μ M MS177, negative controls (MS177-N1 and MS177-N2), C24 or DMSO vehicle control for 48 h, (2) 2.5 μ M MS8815, negative control (MS8815-N), EPZ-6438 or DMSO vehicle control for 30 h. Strikingly, the transcriptome-wide gene expression changes induced by

MS8815 and MS177 were highly significantly correlated, and significantly correlated with gene expression changes induced by MS177 in T47D cells (Fig. 3D,E). Similarly, the genes significantly upregulated and downregulated by MS8815 and MS177 treatment in T47D-TR showed a strong overlap with the genes differentially expressed in response to MS177 treatment in T47D cells (Fig. 3F; complete list in Supplemental Table 1), and demonstrated significantly reduced gene expression changes in response to treatment with methyltransferase inhibitors or negative controls (Fig. S2E, F). Analysis of data obtained from DepMap [35] revealed that the genes downregulated by EZH2 PROTAC treatment in both T47D and T47D-TR cells (184 genes) demonstrated a significant association of being more essential for luminal A BC cell line growth; a less significant opposite association was noticed for upregulated genes (174) (Fig. S2G). Together, these data suggest potent on-target transcriptomic effects of MS177 and MS8815 treatment in luminal BC cells. Moreover, normalized enrichment scores (NES) from GSEAs of HALLMARK gene sets showed a significant correlation between MS8815 and MS177 treatment in T47D-TR cells, and cell cycle related gene sets were among those negatively associated with both treatments (Fig. 3G); similarly, both E2F and FOXM1 direct targets were significantly negatively associated as well (Fig. 3H). Similar to the data obtained from T47D cells, these data show that MS177 and MS8815 treatment reduces the expression of cell cycle-related genes and inhibits the growth of the tamoxifen-resistant T47D-TR cells.

EZH2 binds to the promoters of FOXM1 target genes independent of estrogen signaling

Because our lab and others have shown noncanonical coactivator functions of EZH2 with several transcription factors in a variety of cancer types [20, 22–24, 36], and that EZH2-targeted PROTAC treatment inhibits the growth of luminal BC cells to a much larger degree compared to the corresponding methyltransferase inhibitors, we sought to determine the genomic location of EZH2 binding, with a special emphasis on regions without the EZH2-PRC2-catalyzed H3K27me₃ repressive mark. To this end, Cleavage Under Targets and Release Using Nuclease (CUT&RUN) or Cleavage Under Targets and Tagmentation (CUT&Tag) were employed for mapping EZH2, H3K27me₃ and H3K27ac (an activating histone mark). Additionally, because EZH2 has been reported to be a coactivator of ER [25], both T47D and BT-549 (a TNBC cell line) cells were profiled in order to determine the extent of differences in EZH2 binding in BC cell lines with and without ER expression. As expected, and in both cell lines, regions with EZH2 binding peaks in the absence of H3K27me₃ (EZH2_solo peaks) exhibited increased signals of H3K27ac and ATAC-seq [37], suggestive of transcriptionally active and accessible chromatin regions (Fig. 4A, B). Similarly, and in both cell lines, EZH2 signal correlated with H3K27me₃, H3K27ac and ATAC-seq signal, while H3K27me₃ only demonstrated a strong positive correlation with EZH2 signal (Fig. 4C, D). Additionally, EZH2 signal positively



correlated between T47D and BT-549 cells ($R = 0.47$) (Fig. S3A). EZH2_solo peaks demonstrated a strong overlap with both H3K27ac and ATAC-seq peaks in both cell lines (Fig. 4E, F), and EZH2_solo peaks also demonstrated a considerable overlap between T47D and BT-549 cells, with approximately 45% of

T47D EZH2_solo peaks being present in BT-549 cells (Fig. S3B). Annotation of the EZH2_solo peaks showed that approximately half of these peaks were located in the promoter region of genes in both cell lines (Fig. S3C), while H3K27me3 peaks were more associated with intergenic regions (Fig. S3D). ChEA3 analysis [38]

Fig. 3 MS177 and MS8815 inhibit growth and reduce cell cycle regulated gene sets in tamoxifen resistant breast cancer cells. Plots showing relative absorbances from MTS assays of T47D-TR cells treated with labeled concentrations of MS177, controls (MS177-N1, MS177-N2), C24 (A) or MS8815, MS8815-N, EPZ-6438 (B). Relative absorbance numbers presented were calculated relative to cells grown treated with DMSO vehicle control. MTS assays were carried out six days after treatment of labeled compounds. $N = 3$ biological replicates. $*p < 0.05$ comparing EZH2 PROTAC to all other treatments as determined by two-sided t test and Bonferroni's adjustment. Error bars represent mean \pm s.d. Tables are located beneath the plots showing the IC_{50} growth values in T47D-TR cells after six days of treatment. N.D. = Not Determined, ie greater than $5 \mu\text{M}$. C Western blots showing EZH2 and EED protein expression in lysates from T47D-TR cells treated with $2.5 \mu\text{M}$ MS8815, MS8815-N, EPZ-6438 or DMSO vehicle control (Top) or $2.5 \mu\text{M}$ MS177, MS177-N1, MS177-N2, C24 or DMSO vehicle control (Bottom). Cells were treated with labeled compounds for 48 h prior to cell lysis and subsequent western blot analyses. Calnexin was used as a loading control. D 3D Scatter plot showing the correlation of $\log_{2}FC/lfcSE$ numbers for the expression of each gene comparing MS177 vs DMSO and MS8815 vs DMSO as determined by RNA-seq of RNA extracted from T47D and T47D-TR cells treated with $2.5 \mu\text{M}$ MS177 or DMSO for 48 h, and T47D-TR cells treated with $2.5 \mu\text{M}$ MS8815 or DMSO for 30 h. Color indicates mean $\log_{2}FC/lfcSE$ of all three comparisons. E Plot showing r -values for the three comparisons in the 3D scatter plot. $p < 2.2E-16$ for each comparison, which was calculated from r -value. F Venn diagrams showing the number of genes significantly upregulated (Left) and downregulated (Right) in each of the three comparisons. G Scatter plot showing the correlation between NES values from GSEAs using the HALLMARK gene sets, comparing MS177 vs DMSO and MS8815 vs DMSO treatment of T47D-TR cells, as determined by RNA-seq. Blue and red dots indicate gene sets that are significantly (adjusted p values < 0.05) negatively and positively associated with MS177 and MS8815 treatment. Specific gene sets of interest, such as negatively associated cell cycle related gene sets, are labeled. H Ridge plots showing the Fischer cell cycle gene sets [33] significantly negatively and positively (adjusted p value < 0.05) associated with MS177 and MS8815 treatment of T47D-TR compared to DMSO control as determined by GSEAs with RNA-seq results.

(which combines publicly available CHIP-seq, co-expression and co-occurrence data, and gene expression changes in response to transcription factor perturbations to identify transcription factor targets) identified three common transcription factors highly associated with genes paired with the EZH2_solo bound promoters between the two cell lines, including FOXM1 (Fig. 4G). FOXM1 is a transcription factor that plays an important role in activating genes involved in regulating G2/M phases of the cell cycle [39]. And G2M checkpoint associated-transcripts and FOXM1 target genes were found to be downregulated by MS177 treatment in T47D cells, and by MS8815 and MS177 treatment in T47D-TR cells (see Figs. 2, 3). While specific genes associated with H3K27me3 and EZH2 peaks in intergenic and promoter regions were largely void of H3K27ac or ATAC-seq signal (Fig. S3E), several FOXM1 target genes, including AURKB, TPX2, TOP2A, UBE2T, NEK2 and ECT2, exhibited strong co-occupancy of EZH2, H3K27ac and ATAC-seq read density, as well as a lack of H3K27me3, within respective promoter regions in both T47D and BT-549 cells (Figs. 4H, S3F); of note, these genes were downregulated by EZH2 PROTAC treatment in T47D cells. Genes associated with EZH2_solo bound promoters (EZH2_solo genes) showed a significant overlap between T47D and BT-549 cells (1673 total genes, $p < 2.2E-16$), and these genes also significantly overlapped with FOXM1 target genes, with 45 genes being in all three lists (Fig. 4I). Additionally, EZH2_solo-associated genes in T47D cells significantly overlapped with genes downregulated, but not upregulated, by MS177, as determined by RNA-seq (Fig. 4J, upper). Likewise, H3K27me3-associated genes in T47D cells significantly overlapped with genes upregulated, but not downregulated, by MS177 (Fig. 4J, bottom). These results suggest that many of these genes, including FOXM1 target genes, may be directly regulated by EZH2 and therefore directly reduced by EZH2-targeted PROTAC treatment.

Because of the high degree of overlap between EZH2_solo genes in T47D and BT-549 cells, cell growth and RNA-seq transcriptomic analyses were carried out in TNBC cells in response to MS177 treatment. Similar to what was seen in the tested luminal BC cell lines, MS177 treatment: (1) decreased the growth of BT-549, MDA-MB468 and HCC1143, which are all human TNBC cell lines (Fig. S4A–C), (2) resulted in reductions in EZH2 and EED protein levels (Fig. S4D–F), (3) resulted in significantly differentially expressed genes that showed minimal changes with MS177-N1, MS177-N2 or C24 treatment in BT-549 cells (Fig. S4G, complete list in Supplementary Table 1) and reduced the expression of FOXM1 targets and cell cycle related HALLMARK gene sets (Fig. S4H, I). Additionally, GSEAs with gene sets comprised of genes significantly downregulated (184 genes) and upregulated (174 genes) by EZH2-

targeted PROTACs in T47D and T47D-TR (see Fig. 3D) showed significant negative and positive associations with MS177 treatment in BT-549 cells, respectively (Fig. S4J, K). However, EZH2_solo and H3K27me3 associated genes in BT-549 cells did not demonstrate similar significant overlaps with genes differentially expressed in response to MS177, as seen in T47D cells (Fig. S4L). Interestingly, many FOXM1 target and cell cycle related genes still showed significant p values, but failed to reach the used threshold of $\log_{2}FC < -1$, in response to MS177 treatment of BT-549 cells (data not shown); perhaps explaining the poor overlap between EZH2_solo and MS177 downregulated genes. Together, these data show that the location of EZH2 binding in active chromatin shows some similarity between luminal BC and TNBC cells and these binding sites are significantly associated with FOXM1 targets, independent of ER expression. Furthermore, FOXM1 target genes are among the genes downregulated by EZH2-targeted PROTAC treatment in both luminal BC and TNBC cell lines.

EZH2 physically interacts with FOXM1 in luminal BC cells and MS177 and MS8815 reduce FOXM1 protein levels

Since EZH2 was found to bind to FOXM1 target genes and EZH2-targeted PROTACs were found to reduce FOXM1 target gene expression, we chose to test for EZH2/FOXM1 physical interaction and proximity in T47D cells. Firstly, exogenous HA-tagged EZH2 was overexpressed in T47D cells, and FOXM1 and EED (PRC2 positive control) were both immunoprecipitated from lysate with anti-HA bound beads but not with the mouse IgG negative control, as detected by western blot (Fig. 5A). This suggests that EZH2 physically interacts with FOXM1 in T47D cells. To further confirm the close proximity of EZH2 and FOXM1 within T47D cells, a BirA*-EZH2 fusion protein was overexpressed in T47D cells (Fig. 5B) and streptavidin beads were used to pull-down biotin-labeled proteins from cell lysates of cells grown in the presence and absence of 50 μM biotin for 24 h. Western blot analyses showed that EZH2, EED and FOXM1 were pulled down in higher amounts from lysates obtained from biotin-treated cells compared to those grown in the absence of biotin; however, GAPDH (negative control) was not detected in streptavidin pull-down samples (Fig. 5B), suggesting that FOXM1 can be biotin labeled via BirA*-EZH2, and that EZH2 and FOXM1 therefore exist in close proximity in T47D cells. Furthermore, MS177 and MS8815 treatment resulted in reduced FOXM1 protein expression in T47D, T47D-TR and CAMA1 cells, as determined by western blot, while similar reductions were not seen in response to treatment with corresponding methyltransferase inhibitors or negative controls (Fig. 5C, D and S5A). Similar results were also obtained with the TNBC cell lines BT-549, MDA-MB-468 and HCC1143

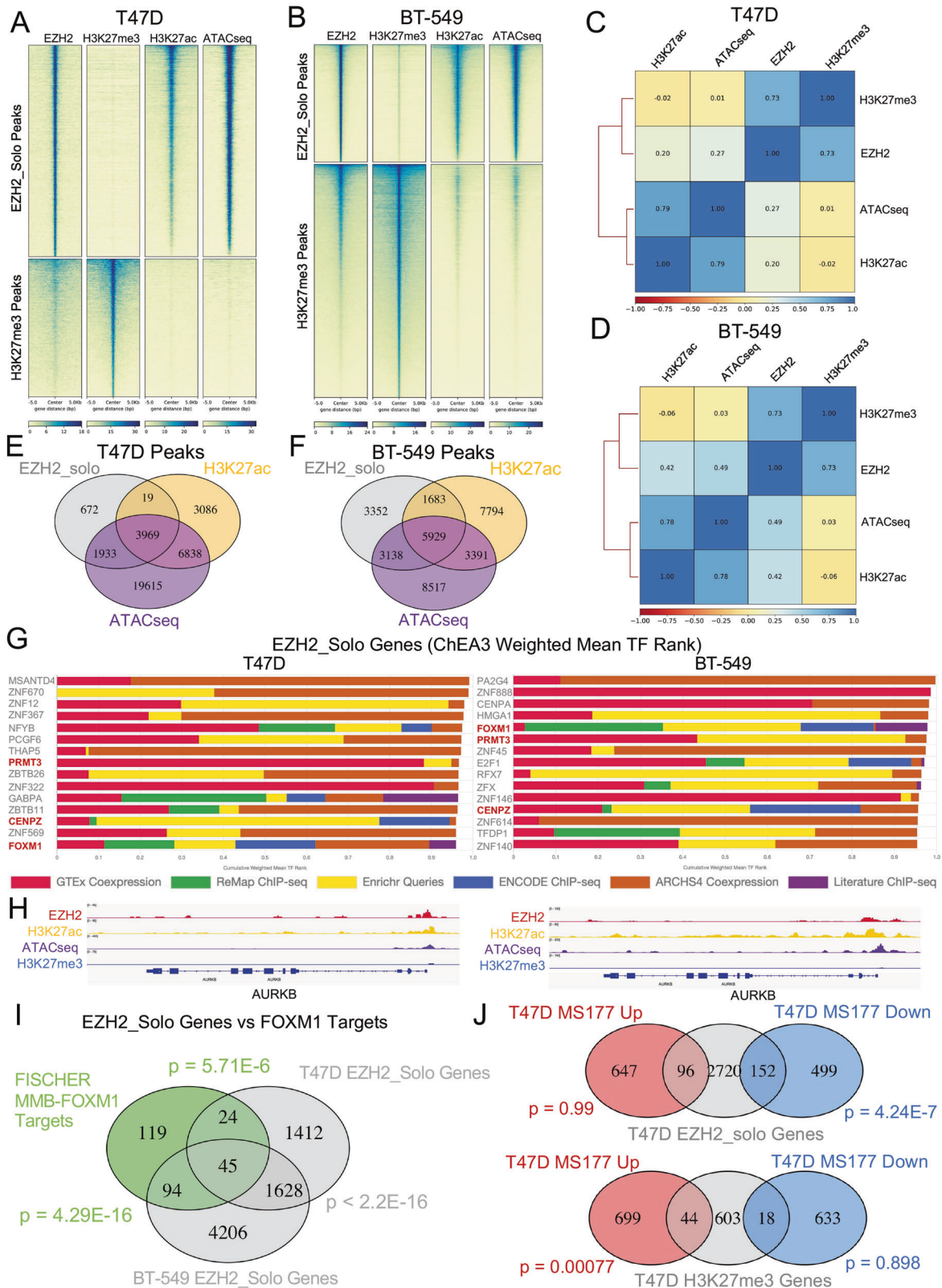


(Fig. S6A–C). FOXM1 protein levels exhibited dose-dependent reductions in response MS177 and MS8815 treatment of T47D cells (Fig. 5E). Similarly, FOXM1 target genes exhibited significant negative associations with EZH2 PROTAC treatment compared to the negative controls or methyltransferase inhibitors, as

determined by GSEA from RNA-seq results of T47D, T47D-TR and BT-549 cells (Fig. 5F, G, S5B–G and S6D–F). Furthermore, reductions in FOXM1 protein levels correlated with increased FOXM1 degradation in response to MS177 treatment, as determined by cycloheximide time-course and western blot

Fig. 4 **EZH2 solo binding sites are associated with FOXM1 target gene promoters.** Heatmaps showing the CUT&RUN and CUT&Tag EZH2, H3K27me3 and H3K27ac and ATAC-seq [37] intensities at \pm 5 kb surrounding EZH2 solo peaks (EZH2 peaks independent of H3K27me3) and H3K27me3 peaks in T47D (A) and BT-549 (B) cells. Correlation plots showing the correlations of read distribution between EZH2, H3K27me3, ATAC-seq and H3K27ac in T47D (C) and BT-549 (D) cells. Venn diagram showing the overlap of EZH2_solo, H3K27ac and ATAC-seq peaks in T47D (E) and BT-549 (F) cells. G ChEA3 Weighted Mean TF Rank from lists of genes with EZH2 solo peaks within promoter regions (EZH2_solo genes) in T47D (Left) and BT-549 (Right) cells. H IGV tracks showing the CUT&RUN and CUT&Tag read densities for EZH2, H3K27ac and H3K27me3, as well as ATAC-seq, at the FOXM1 responsive gene, AURKB in T47D (Left) and BT-549 (Right) cells. I Venn diagram showing the overlap of EZH2 solo genes in T47D and BT-549 cells and Fischer FOXM1-MMB target genes [33]. P values calculated by hypergeometric distribution are labeled next to each pairwise overlap. J Venn diagrams showing the overlap of EZH2 solo genes (Top) and H3K27me3 associated genes (Bottom) in T47D cells and genes upregulated (red) and downregulated (blue) by MS177 in T47D cells as determined by RNA-seq. P values calculated by hypergeometric distribution are labeled next to each pairwise overlap.

analysis in T47D cells (Fig. 5H), suggesting that EZH2-targeted PROTACs are able to target interacting EZH2 and FOXM1 proteins for degradation. These results suggest that EZH2 physically interacts with FOXM1 in T47D cells, and that EZH2-targeted PROTACs, not EZH2 methyltransferase inhibitors, reduce EZH2 and FOXM1 protein expression and FOXM1 target gene expression.

EZH2 mRNA expression positively correlates with FOXM1 and target genes in luminal A and triple negative breast cancers

In order to gain insight into the clinical relevance of EZH2 and FOXM1 target gene regulation in luminal BC, mRNA expression data from LumA BC and TNBC patients within the publicly available METABRIC and TCGA cohort studies were analyzed. Firstly, FOXM1 and EZH2 mRNA expression were found to be highly significantly correlated in both BC subtypes (Fig. 6A, S7A and S8A, B), and both genes exhibited significantly higher expression in TNBC (Fig. S8C, D). In support of previous reports which found high FOXM1 expression to be associated with worse prognosis specifically in luminal BC, but not TNBC [28], we found that high expression of both EZH2 and FOXM1 was only significantly associated with decreased relapse-free and disease-free survival in LumA BC patients (Figs. 6B, S7B). GSEA using transcriptome-wide r-values of gene expression correlations with EZH2 showed that EZH2 positively correlates with cell cycle related HALLMARK gene sets, FOXM1 targets and tamoxifen resistance associated genes (Fig. 6C–E and S7C–E), thus mirroring our transcriptomic analyses of T47D and T47D-TR cells in response to EZH2-targeted PROTAC treatment, which showed downregulation of said gene sets (See Figs. 2, 3). Similar significant positive correlations between EZH2 and FOXM1 target gene expression was found with TNBC patient samples (Fig. S8E, F). Additionally, genes significantly upregulated and downregulated by EZH2-targeted PROTAC treatment in T47D and T47D-TR cells were negatively and positively correlated with EZH2 expression in LumA BC clinical samples, respectively (Fig. 6F, G and S7F, G). These data suggest that EZH2-targeted PROTACs target a clinically relevant EZH2-FOXM1 axis of gene expression regulation in tamoxifen naive and resistant LumA BC and TNBC cells.

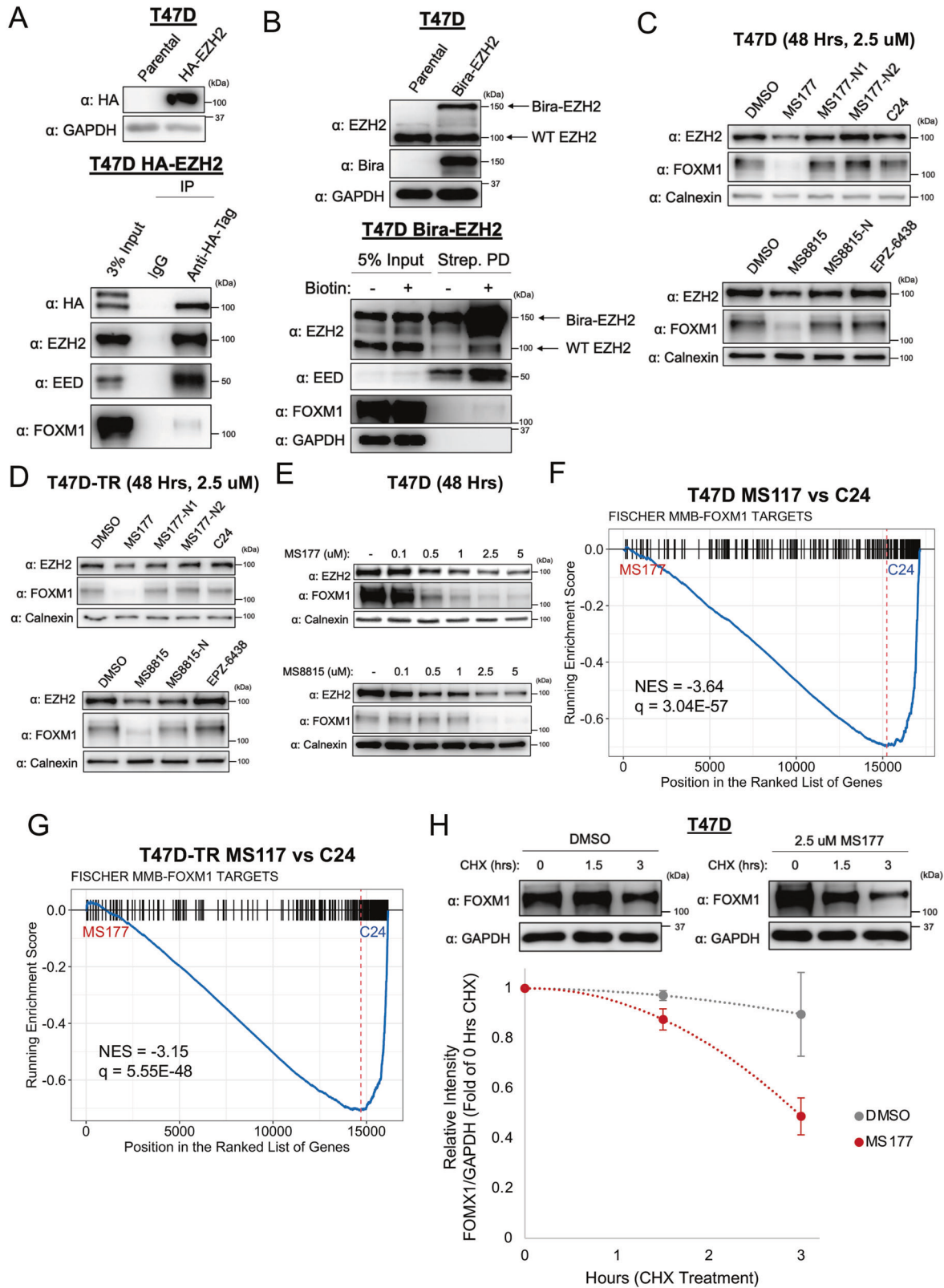
DISCUSSION

Growing evidence points to important coactivator functions of EZH2 in addition to its methyltransferase and PRC2-dependent canonical role as transcription repressor [20, 22–24, 36]. Several transcription factors with which EZH2 functions as a coactivator play vital roles in cancer progression, including MYC, AR, and E2F1 [20, 22, 23, 26], suggesting that these are important mechanisms through which EZH2 drives oncogenesis. Because many of the coactivator functions of EZH2 are methyltransferase-independent and PRC2-independent, EZH2 methyltransferase inhibitors fail to target vital oncogenic roles of EZH2 in cancer cells. These shortcomings of EZH2 methyltransferase inhibitors are potentially overcome through the development of EZH2 targeted PROTACs. EZH2-targeted PROTACs can effectively degrade EZH2, in addition

to interacting proteins, including proteins involved in both PRC2-dependent and PRC2-independent interactions; therefore, PROTACs offer the advantage of blocking both repressor and coactivator functions of EZH2. In fact, in this study we present data suggesting that EZH2-targeted PROTACs, MS177 and MS8815, effectively reduce the protein levels EZH2 and FOXM1 and inhibit the cell growth of BC cells; including cells resistant to tamoxifen, which presents a significant challenge in the clinical management of luminal BC. Genomic and transcriptomic analyses suggest that the PROTAC-mediated reductions in FOXM1 target gene expression are independent of ER expression and is a phenomenon in both luminal BC and TNBC. This possibility makes these PROTACs attractive potential therapeutic strategies to overcome tamoxifen resistance, since estrogen-independent mechanisms of cell cycle progression, such as CCND1 amplification and high MYC and FOXM1 expression, have been implicated in tamoxifen resistance [28, 40, 41].

We found that EZH2-targeted PROTACs effectively reduced the growth of the tamoxifen-resistant T47D-TR cells. A previous study by Wu et al. [14] found that EZH2 promotes tamoxifen resistance through the PRC2-mediated repression of GREB1, which in turn modulates ER coregulator distribution and promotes ER activity in the presence of tamoxifen. The interactions between EZH2 and transcription factors known to be implicated with reduced relapse free survival in luminal BC, such as FOXM1 [28], may point to multiple of mechanisms of EZH2 mediated tamoxifen resistance that should be explored. Interestingly, we found that while EZH2 and FOXM1 mRNA expression is significantly higher in TNBC samples compared to LumA BC, high EZH2 and FOXM1 mRNA expression was only significantly associated with reduced relapse free and disease-free survival in LumA BC. This trend has been reported for FOXM1 mRNA expression in BC samples [28] and may suggest that LumA BC cells with higher FOXM1 and EZH2 mRNA expression mark cells with a growth advantage, especially in the setting of therapeutic intervention, such as tamoxifen treatment.

A previous study by Mahara et al. [27] showed data demonstrating that hypoxia-inducible factor (HIF1a) directly suppresses SUZ12 and EED in TNBC, leading to a functional switch of EZH2 from a repressor to an activator of MMPs in cooperation with FOXM1 during hypoxic conditions. Interestingly, the HIF1a-mediated repression of EED and SUZ12 was not seen in luminal BC cell lines in this study. Multiple studies in different cancer types have found that the phosphorylation of EZH2 by a variety of kinases, including, AKT, AMPK and JAK3, can lead to the dissociation of EZH2 from PRC2 and promote its coactivator functions [15, 20, 42–44]. Specifically, phosphorylation of EZH2 at serine 21 was found to unmask a cryptic partially disordered transactivation domain (TAD), which subsequently interacts with the transcription activator, p300 histone acetyltransferase [44]. Other studies have implicated the phosphorylation of serine 21 or TAD of EZH2 in mediating interactions with, and coactivation of, MYC and the AR [20, 22, 23]. Therefore, while the HIF1a-mediated EZH2/FOXM1 interaction does not



seem to occur in luminal BC, it is quite possible that other mechanisms, such as phosphorylation could be at play. In fact, the physical interaction and proximity experiments in the study were carried out in normoxic conditions. Therefore, future studies are needed to delineate the nature of the EZH2/FOXM1

interaction and the regulatory mechanisms that promote the noncanonical activities of EZH2, including its interaction with FOXM1, in different BC subtypes.

While we found that EZH2 binds to FOXM1 target gene promoters, and that EZH2-targeted PROTACs reduce FOXM1 protein

Fig. 5 EZH2 physically interacts with FOXM1 in ER+ breast cancer cells and EZH2 targeted PROTACs reduce FOXM1 protein and target gene expression compared to methyltransferase inhibitors and negative controls. **A** Western blots showing expression of HA-tagged EZH2 (HA-EZH2) in lysates from T47D cells with stably expressed HA-EZH2 compared to parental cells. GAPDH was used as loading control (Top). Western blots showing HA-tagged EZH2, endogenous EZH2, EED and FOXM1 expression in input lysate and proteins immunoprecipitated using normal IgG and anti-HA antibodies (Bottom). **B** Western blots showing EZH2 and BirA*-EZH2 protein expression in lysates from T47D cells expressing BirA*-EZH2 recombinant fusion protein compared to parental cells. Top band in EZH2 blot is the BirA-EZH2 fusion protein (~150 kd), while endogenous wild-type (WT) EZH2 is the bottom band (~100 kd). GAPDH was used as loading control (Top). Western blot showing expression of EZH2 (endogenous and BirA*-EZH2), EED and FOXM1 in input lysate and proteins pulled down by streptavidin agarose beads (Strep. PD) from lysates from T47D cells expressing BirA*-EZH2 and grown in the presence and absence of 50 μ M Biotin. GAPDH was used as a loading control for input lysate (Bottom). Western blots showing EZH2 and FOXM1 protein expression in lysates from T47D (C) and T47D-TR (D) cell lines treated with 2.5 μ M MS177, MS177-N1, MS177-N2, C24 or DMSO vehicle control (Top) or 2.5 μ M MS8815, MS8815-N, EPZ-6438 or DMSO vehicle control (Bottom). Cells were treated with labeled compounds for 48 h prior to cell lysis and subsequent western blot analyses. Calnexin was used as loading control. **E** Western blots showing EZH2 and FOXM1 protein expression in lysates from T47D cells treated with labeled concentrations of MS177 (Top) or MS8815 (Bottom) or DMSO vehicle control for 48 h prior to cell lysis and subsequent western blot analyses. Calnexin was used as a loading control. Enrichment plots showing enrichment of the Fischer et al. MMB-FOXM1 target gene set [33] in T47D (F) and T47D-TR (G) cells treated with MS177 compared to C24, as determined by GSEAs from RNA-seq results. *P* values were adjusted using FDR, and *q* values < 0.05 were considered significant. **H** Top panel: Western blots showing FOXM1 levels in lysates from T47D cells treated with 2.5 μ M MS177 or DMSO for 3 h followed by 0, 1.5 or 3 h of 100 μ g/ml cycloheximide along with DMSO or 2.5 μ M MS177. GAPDH was used as loading control. Bottom panel: Graph showing the relative intensity of FOXM1 relative to GAPDH at each time point relative to 0 h cycloheximide treatment for both DMSO and MS177 treatments. The experiment was repeated twice with the representative results shown here. Error bars represent mean \pm s.d. Relative intensities were calculated using ImageJ.

levels and FOXM1 target gene expression, it is likely that EZH2 interactions with other cell cycle transcription factors also play a role in the growth inhibitory effects of EZH2-targeted PROTACs. A previous study from our group found that EZH2 targeted PROTACs were capable of degrading the EZH2/MYC complex [22]. Another study found that EZH2 shelters MYC from ubiquitin ligases through its physical interaction [45]. There may therefore be multiple mechanisms through which EZH2 targeted PROTACs cause MYC degradation in cancer cells. EZH2 has also been proposed to function as a coactivator of E2F1 [26]. Interestingly, in addition to MYC, which is a vital cell cycle regulator, E2F transcription factors and FOXM1 are central regulators the G1/S and G2M cell cycle transitions, respectively; therefore, it is possible that EZH2 plays important coactivator roles throughout cell cycle progression in cancer cells. Additionally, EZH2 can also regulate the cell cycle through PRC2-mediated repression of tumor suppressors [9]. Together, this growing body of evidence would suggest a multitude of canonical and noncanonical mechanisms through which EZH2 regulates cell cycle progression; therefore, the potential ability to target a regulator of multiple points of the cell cycle make EZH2 targeted PROTACs intriguing potential therapeutics in BC and other cancer types. Together with previous studies, this study underscores the advantage of EZH2-targeted PROTACs over methyltransferase inhibitors as potential therapeutic modalities in different BC subtypes, including tamoxifen resistant luminal BC.

MATERIALS AND METHODS

Cell culture

T47D, CAMA1, T47D-Tam1 (T47D-TR), BT-549, HCC1143, MDA-MB-468 and HEK293T cell lines were obtained from American Type Culture Collection (ATCC). T47D, T47D and BT-549 cell lines were maintained in RPMI 1640 medium (Gibco) supplemented with 10% fetal bovine serum (FBS) (Corning), 100 units/mL penicillin, 100 μ g/mL streptomycin and 8 μ g/ml human recombinant insulin (Gibco). In addition, T47D-TR cells were maintained in growth media containing 1 μ M tamoxifen to maintain resistance to tamoxifen. The HCC1143 cell line was maintained in RPMI 1640 medium (Gibco) supplemented with 10% FBS (Corning), 100 units/mL penicillin and 100 μ g/mL streptomycin. CAMA1, MDA-MB-468 and HEK293T cell lines were maintained in DMEM (Gibco) supplemented with 10% FBS (Corning), 100 units/mL penicillin and 100 μ g/mL streptomycin. Identity of cell lines was validated through genetic signature analyses and mycoplasma contamination was tested routinely using commercial detection kits (Lonza, #LT27-286).

Chemicals

MS177, MS177-N1, MS177-N2, C24, MS8815, MS8815-N and EPZ-6438 were synthesized as previously described [22, 31]. Tamoxifen (Sigma-Aldrich, T2859) and cycloheximide (Sigma-Aldrich, 01810) were purchased from Sigma-Aldrich.

Transductions and stable cell lines

T47D cells with stable expression of HA-EZH2 were generated by transducing T47D cells with lentiviral particles packaged with the pCDH-EF1-MCS-IRES-neo vector (System Biosciences) with HA-tagged EZH2 cloned in, as previously described [22], and positive cells were selected by G418 treatment. T47D cells with stable expression of BirA*-EZH2 were generated by transducing T47D cells with retroviral particles packaged with MSCV-puro vector with BirA*-EZH2 fusion cDNA cloned in, and positive cells were selected by puromycin treatment. Lentiviral and retroviral particles were generated by transfecting HEK-293T cells with plasmids of interest and psPAX2 and CMV-VSVG or pCL-10A1, respectively, using Lipofectamine 3000 Reagents (Invitrogen, L3000075).

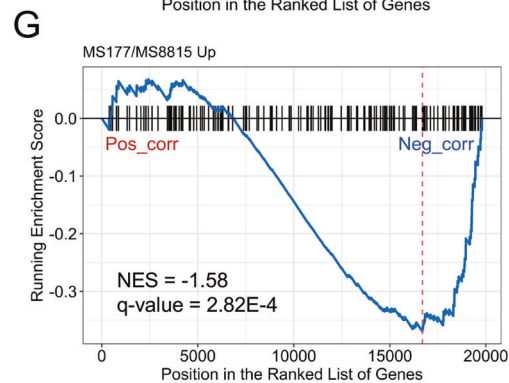
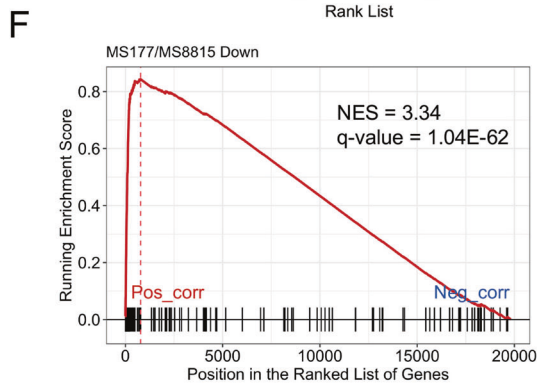
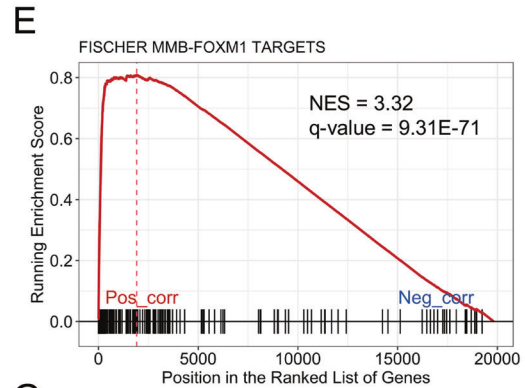
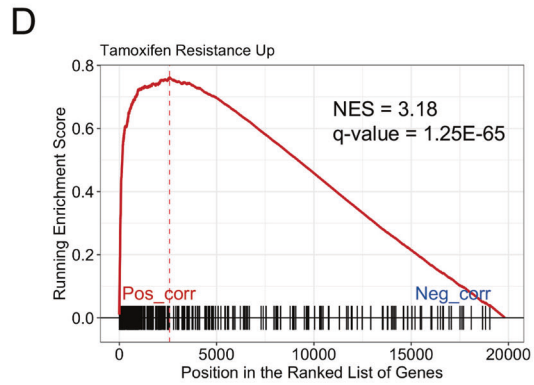
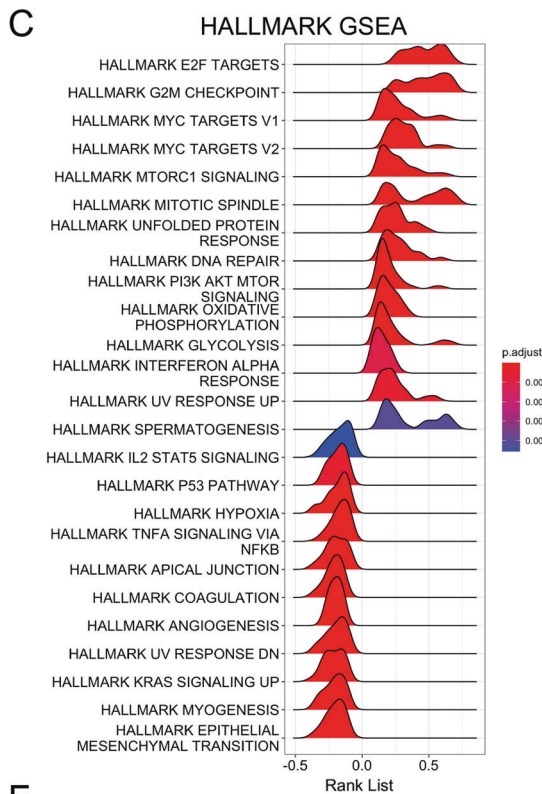
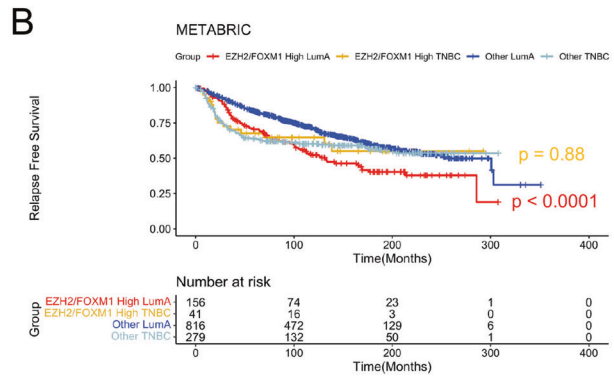
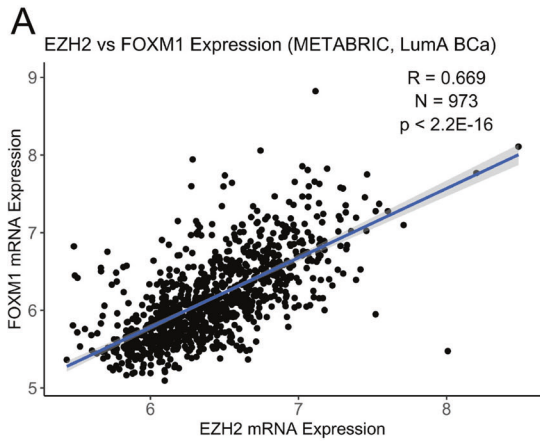
Cell growth and colony formation assays

For cell growth assays, T47D, CAMA1 and T47D-TR cells were seeded in 96-well plates at a density of 3,000 cells per well, while HCC1143, MDA-MB-468 and BT-549 cells were seeded at a density of 500 cells per well. After allowing cells to attach for 18 h, cells were treated EZH2-targeted PROTACs (MS177 and MS8815), methyltransferase inhibitors (C24 and EPZ-6438), negative controls (MS177-N1, MS177-N2, MS8815-N) or DMSO vehicle control. Media was refreshed every 48 h to maintain drug concentration. Colorimetric MTS assay was utilized as a surrogate for cell number using the CellTiter 96 AQueous One Solution Cell Proliferation Assay (MTS) (Promega, G3582). Relative absorbance to DMSO vehicle control treated cells was calculated to determine the anti-growth effects of the compounds. Significance between groups, when tested, was determined via *t* test, with *n* \geq 3 for each group to ensure statistical power to ensure statistical power; however, no statistical methods were used to pre-determine sample size.

For colony formation assays, T47D and T47D-TR cells were seeded in 6-well plates at a density of 500 cells per well. Cells were allowed to attach for 18 h and then were treated with EZH2-targeted PROTACs (MS177 and MS8815), methyltransferase inhibitors (C24 and EPZ-6438), negative controls (MS177-N1, MS177-N2, MS8815-N) or DMSO vehicle control; for tamoxifen experiments, ethanol was used as a vehicle control. After a sufficient number of colonies grew in control plates, the plates were washed in PBS, fixed in methanol for 10 min and stained with crystal violet.

Western blot

Cells were treated as described in the results section and figure legends and were lysed by boiling in SDS sample buffer. Proteins were then separated by SDS-PAGE in 10% acrylamide SDS gels. Proteins were transferred to 0.2 μ M PVDF membranes (BioRad, #1620177) overnight at 4 $^{\circ}$ C. Incubation in 5% NFDm for 1 h was used for blocking, and membranes were incubated in primary antibodies in 5% NFDm overnight at 4 $^{\circ}$ C. The following antibodies and dilutions were used: EZH2 1:1000 (Cell Signaling Technology, #5246), EED 1:1000 (Cell Signaling Technology, #85322), SUZ12 1:1000 (Cell Signaling Technology, #3737), FOXM1 1:500 (Cell Signaling Technology, #20459),



H3K27me3 1:1000 (Cell Signaling Technology, #9733), H3K27me3 1:1000 (Millipore, #07-449), H3 (Cell Signaling Technology, #4499), Calnexin (Cell Signaling Technology, #2433). After washing, membranes were incubated in HRP-conjugated anti-Rabbit (Cell Signaling Technology, #7074) and anti-Mouse (Cell Signaling Technology, #7076)

secondary antibodies in 1:2000 5% NFDN for 1 h at room temperature. Membranes were then washed and chemiluminescence was detected using Clarity Western ECL Substrate (BioRad, 1705061) or SuperSignal West Femto Maximum Sensitivity Substrate (ThermoFischer, 34094).

Fig. 6 EZH2 mRNA expression correlates with FOXM1, FOXM1 target genes, cell cycle regulated gene sets, and genes associated with tamoxifen resistance in luminal A BC clinical samples from the METABRIC study. **A** Scatter plot showing correlation between EZH2 and FOXM1 mRNA expression from luminal A BC samples from the METABRIC study [50, 51] ($N = 973$). **B** Kaplan-Meier plot showing the relapse free survival of luminal A BC and TNBC patients from the METABRIC study stratified by EZH2 and FOXM1 high mRNA expression (higher than 75th percentile for both genes, LumA $N = 156$, TNBC $N = 41$) and all other patient samples for each subtype (LumA $N = 816$, TNBC $N = 279$). P values for each subtype were calculated by log-rank test. **C** Ridge plots showing HALLMARK gene sets with significant negative and positive associations – as determined by GSEA—with genes rank ordered by Spearman correlation r -values with EZH2 mRNA expression within luminal A BC samples from the METABRIC study. Enrichment plots from GSEAs using gene sets comprised of genes associated with tamoxifen resistance [34] **(D)** FOXM1 target genes [33] **(E)** and genes downregulated **(F)** and upregulated **(G)** by EZH2 PROTAC treatment in T47D and T47D-TR cell lines, as determined by RNA-seq (see Fig. 3E). Genes were rank ordered as stated above in 6 C. P values were adjusted by FDR (q -value) and $q < 0.05$ was considered significant.

Co-immunoprecipitation and proximity dependent biotin identification (BioID)

For immunoprecipitation, the manufacturer protocol (<https://www.thermofisher.com/order/catalog/product/11201D>) was followed. Cells were grown in 10 cm plates and were lysed on ice using EBC buffer with protease inhibitor cocktail for 30 min, followed by centrifugation at 14,000 g for 15 min at 4 °C to remove cellular debris. Mouse anti-HA (Roche, 12CA5) and normal mouse IgG (Millipore, CS20062) were bound to Dynabeads M-280 Sheep anti-Mouse IgG beads (Invitrogen, 11201D), and antibody coated beads were incubated with lysates overnight at 4 °C. After washing, immunoprecipitated proteins were removed from antibody coated beads by boiling in SDS sample buffer.

For BioID, T47D BirA*-EZH2 cells were grown in 15 cm plates in the presence and absence of 50 μ M biotin for 24 h. After biotin treatment, cells were lysed on ice using RIPA buffer with protease inhibitor cocktail, followed by the addition of benzonase and 1 h incubation on ice to degrade DNA. Samples were snap frozen and thawed on ice, followed centrifugation at top speed for 30 min at 4 °C to pellet debris. NeutrAvidin Agarose beads (Thermo Scientific, 29204) were washed in RIPA buffer, and then incubated with lysates overnight at 4 °C. After washing beads with RIPA and TAP lysis buffers, bound proteins were removed from beads by boiling in SDS sample buffer.

RNA-sequencing (RNA-seq) and data analysis

RNA-seq was performed as previously described [22, 23]. T47D, T47D-TR and BT-549 cells were treated with 2.5 μ M MS177, MS177-N1, MS177-N2, C24 or DMSO control for 48 h prior to RNA extraction. T47D-TR cells were treated with 2.5 μ M MS8815, MS8815-N, EPZ-6438 or DMSO control for 30 h prior to RNA extraction. Experiments were carried out with two repeats per condition to ensure statistical power; however, no statistical methods were used to pre-determine sample size. Total RNA was extracted using the RNeasy Plus Mini Kit (Qiagen, #74136). On-column DNA digestion or gDNA Eliminator columns were used to remove genomic DNA. Isolation of mRNA was conducted using Oligo dT Beads and multiplexed cDNA libraries were generated using NEBNext Ultra II RNA Library Prep Kit for Illumina (New England BioLabs, #E77705). Sequencing was carried out using Illumina Next-Generation sequencer at a sequence depth of 10–20 million reads. Resulting fastq files were aligned to the GRCh38 human genome using STAR, and DESeq2 was used for differential gene expression analyses. Differential gene expression was calculated for treatment relative to DMSO vehicle control for each comparison. Gene set enrichment analysis (GSEA) was conducted using the clusterProfiler R package [46], and HALLMARK gene sets (MSigDB) were obtained using the msigdb package. Gene sets of tamoxifen resistance and Fischer et al. FOXM1 targets [33, 34] were obtained from publicly available data; Fischer et al. gene sets are found within curated (C2) gene sets (MSigDB), and the tamoxifen resistance up gene set was created from genes upregulated in tamoxifen resistant BC samples from 3 separate studies [34]. For GSEA, genes were rank ordered by mean log₂ fold change divided by log₂ fold change standard error (log₂FC/lcSE) for the rank metric, and p values were adjusted by FDR. Ridge plots and enrichment plots were generated using ggridges and enrichplot packages, respectively.

Cleavage under targets and release using nuclease (CUT&RUN) and cleavage under targets and tagmentation (CUT&Tag)

CUT&RUN and CUT&Tag experiments were carried out as previously described [22, 23, 47–49], using EpiCypher CUTANA reagents and following the manufacturer protocols. Antibodies used for CUT&RUN/CUT&Tag: anti-

EZH2 (Cell Signaling Technology, #5246), anti-H3K27me3 (Cell Signaling Technology, #9733), anti-H3K27ac (Cell Signaling Technology, #8173).

Briefly, for CUT&RUN experiments (T47D: EZH2, H3K27me3; BT-549: EZH2, H3K27me3, H3K27ac), T47D and BT-549 cell lines were fixed using 0.1% formaldehyde in 10 cm plates for 1 min, followed by quenching with 20 mM glycine. 5×10^5 cells were then washed and bound to activated concanavilin A (ConA) beads. The cell:bead complexes were then incubated with the antibodies above (1:100 dilution in antibody buffer) overnight at 4 °C and digitonin was used to permeabilize the cells. Cells were then washed followed by incubation with pAG-MNase and round of washes. pAG-MNase was then activated by adding calcium and digestions took place at 4 °C for 2 h. Calcium was then chelated using the stop buffer. Chromatin was released through incubation in SDS and proteinase K containing buffer overnight at 55 °C. 5 ng of purified DNA was used for multiplex library construction using the NEBNext Ultra II DNA Library Prep Kit for Illumina (New England BioLabs, #E7645). Sequencing was carried out using Illumina Next-Generation sequencer at a sequence depth of 5–10 million reads.

Briefly, for CUT&Tag experiment (T47D: H3K27ac), nuclei were extracted from 1×10^5 T47D cells. Nuclei were bound to ConA beads, followed by incubation in 1:100 H3K27ac antibody overnight at 4 °C and digitonin was used to permeabilize the nuclei. Nuclei were washed followed by incubation with secondary antibody. After second round of washing, pAG-Tn5 was tethered to antibody-bound chromatin and activated by magnesium. Tagmented chromatin was released and PCR amplified using barcoded Illumina primers for multiplex library creation. Sequencing was carried out using Illumina Next-Generation sequencer at a sequence depth of 5–10 million reads.

CUT&RUN and CUT&Tag sequencing was analyzed as previously described [22, 23, 47–49]. Briefly, sequences were aligned to the GRCh38 human genome using bowtie, followed by cleaning using Samtools, Picard and bedtools. MACS2 was utilized to call peaks and DeepTools was used to generate bigwig files. Heatmaps were generated using deepTools computeMatrix and plotHeatmap functions, and correlation plots were generated using plotCorrelation. Peak annotations were generated using the HOMER annotatePeaks.pl function. Read densities were visualized at specific gene loci using Integrative Genomics Viewer (IGV, Broad Institute).

Publicly available and previously published ATAC-seq data for T47D and BT-549 cell lines were obtained from the Gene Expression Omnibus (GEO) (GSE254216) [37].

Data mining and patient cohort mRNA expression analysis

Survival and mRNA expression data were obtained for samples from METABRIC [50, 51] and TCGA [52, 53] studies using the cBioportal (www.cbioportal.org). R -values for correlations with EZH2 and all genes were obtained using the cBioportal. Genes were rank ordered by r -value (positive correlation to negative correlation) and GSEAs were carried out using clusterProfiler R package [46]. Gene sets were obtained and plots were generated as described in the RNA-sequencing (RNA-seq) and data analysis section of Materials and Methods. For survival analyses, patient samples were stratified by high EZH2 and FOXM1 expression (75th percentile for both genes) and other, and p values were calculated by log-rank test. Survival plots were generated using “survminer” and “survival” R packages.

DATA AVAILABILITY

Raw and processed sequencing files have been submitted to the Gene Expression Omnibus (GEO) database under the accession numbers of GSE270163 and GSE270769.

REFERENCES

- Siegel RL, Giaquinto AN, Jemal A. Cancer statistics, 2024. *CA Cancer J Clin.* 2024;74:12–49.
- Sorlie T. Molecular portraits of breast cancer: tumour subtypes as distinct disease entities. *Eur J Cancer.* 2004;40:2667–75.
- Cancer Genome Atlas N. Comprehensive molecular portraits of human breast tumours. *Nature.* 2012;490:61–70.
- Baranova A, Krasnoselskiy M, Starikov V, Kartashov S, Zhulkevych I, Vlasenko V, et al. Triple-negative breast cancer: current treatment strategies and factors of negative prognosis. *J Med Life.* 2022;15:153–61.
- Kulkarni A, Stroup AM, Paddock LE, Hill SM, Plascak JJ, Llanos AAM. Breast cancer incidence and mortality by molecular subtype: statewide age and racial/ethnic disparities in New Jersey. *Cancer Health Disparities.* 2019;3:e1–e17.
- Yu NY, Iftimi A, You C, Tobin NP, van 't Veer L, Hoadley KA, et al. Assessment of long-term distant recurrence-free survival associated with tamoxifen therapy in postmenopausal patients with luminal A or luminal B breast cancer. *JAMA Oncol.* 2019;5:1304–9.
- Kuss JT, Muss HB, Hoen H, Case LD. Tamoxifen as initial endocrine therapy for metastatic breast cancer: long term follow-up of two Piedmont Oncology Association (POA) trials. *Breast Cancer Res Treat.* 1997;42:265–74.
- Xu B, Konze KD, Jin J, Wang GG. Targeting EZH2 and PRC2 dependence as novel anticancer therapy. *Exp Hematol.* 2015;43:698–712.
- Yu JR, Lee CH, Okusz O, Stafford JM, Reinberg D. PRC2 is high maintenance. *Genes Dev.* 2019;33:903–35.
- Guo Y, Zhao S, Wang GG. Polycomb gene silencing mechanisms: PRC2 chromatin targeting, H3K27me3 'Readout', and phase separation-based compaction. *Trends Genet.* 2021;37:547–65.
- Guo Y, Yu Y, Wang GG. Polycomb repressive complex 2 in oncology. *Cancer Treat Res.* 2023;190:273–320.
- Fan T, Jiang S, Chung N, Ali Khan A, Ni C, Lee CC, et al. EZH2-dependent suppression of a cellular senescence phenotype in melanoma cells by inhibition of p21/CDKN1A expression. *Mol Cancer Res.* 2011;9:418–29.
- Burr ML, Sparbier CE, Chan KL, Chan YC, Kersbergen A, Lam EYN, et al. An evolutionarily conserved function of polycomb silences the MHC class I antigen presentation pathway and enables immune evasion in cancer. *Cancer Cell.* 2019;36:385–401 e388.
- Wu Y, Zhang Z, Cenciari ME, Proietti CJ, Amasino M, Hong T, et al. Tamoxifen resistance in breast cancer is regulated by the EZH2-ERalpha-GREB1 transcriptional axis. *Cancer Res.* 2018;78:671–84.
- Wang J, Wang GG. No easy way out for EZH2: its pleiotropic, noncanonical effects on gene regulation and cellular function. *Int J Mol Sci.* 2020;21:9501.
- Varambally S, Dhanasekaran SM, Zhou M, Barrette TR, Kumar-Sinha C, Sanda MG, et al. The polycomb group protein EZH2 is involved in progression of prostate cancer. *Nature.* 2002;419:624–9.
- Bachmann IM, Halvorsen OJ, Collett K, Stefansson IM, Straume O, Haukaas SA, et al. EZH2 expression is associated with high proliferation rate and aggressive tumor subgroups in cutaneous melanoma and cancers of the endometrium, prostate, and breast. *J Clin Oncol.* 2006;24:268–73.
- Bae WK, Yoo KH, Lee JS, Kim Y, Chung IJ, Park MH, et al. The methyltransferase EZH2 is not required for mammary cancer development, although high EZH2 and low H3K27me3 correlate with poor prognosis of ER-positive breast cancers. *Mol Carcinog.* 2015;54:1172–80.
- Bae WK, Hennighausen L. Canonical and non-canonical roles of the histone methyltransferase EZH2 in mammary development and cancer. *Mol Cell Endocrinol.* 2014;382:593–7.
- Xu K, Wu ZJ, Groner AC, He HH, Cai C, Lis RT, et al. EZH2 oncogenic activity in castration-resistant prostate cancer cells is Polycomb-independent. *Science (New York, NY (Research Support, N.I.H., Extramural Research Support, Non-U.S. Gov't Research Support, U.S. Gov't, Non-P.H.S.)).* 2012;338:1465–9.
- Yu X, Wang J, Gong W, Ma A, Shen Y, Zhang C, et al. Dissecting and targeting noncanonical functions of EZH2 in multiple myeloma via an EZH2 degrader. *Oncogene.* 2023;42:994–1009.
- Wang J, Yu X, Gong W, Liu X, Park KS, Ma A, et al. EZH2 noncanonically binds cMyc and p300 through a cryptic transactivation domain to mediate gene activation and promote oncogenesis. *Nat Cell Biol.* 2022;24:384–99.
- Wang J, Park KS, Yu X, Gong W, Earp HS, Wang GG, et al. A cryptic transactivation domain of EZH2 binds AR and AR's splice variant, promoting oncogene activation and tumorous transformation. *Nucleic Acids Res.* 2022;50:10929–46.
- Hwang C, Giri VN, Wilkinson JC, Wright CW, Wilkinson AS, Cooney KA, et al. EZH2 regulates the transcription of estrogen-responsive genes through association with REA, an estrogen receptor corepressor. *Breast Cancer Res Treat.* 2008;107:235–42.
- Shi B, Liang J, Yang X, Wang Y, Zhao Y, Wu H, et al. Integration of estrogen and Wnt signaling circuits by the polycomb group protein EZH2 in breast cancer cells. *Mol Cell Biol.* 2007;27:5105–19.
- Xu H, Xu K, He HH, Zang C, Chen CH, Chen Y, et al. Integrative analysis reveals the transcriptional collaboration between EZH2 and E2F1 in the regulation of cancer-related gene expression. *Mol Cancer Res.* 2016;14:163–72.
- Mahara S, Lee PL, Feng M, Tergaonkar V, Chng WJ, Yu Q. HIFI-alpha activation underlies a functional switch in the paradoxical role of Ezh2/PRC2 in breast cancer. *Proc Natl Acad Sci USA.* 2016;113:E3735–3744.
- Lu XF, Zeng D, Liang WQ, Chen CF, Sun SM, Lin HY. FoxM1 is a promising candidate target in the treatment of breast cancer. *Oncotarget.* 2018;9:842–52.
- Zimmerman SM, Lin PN, Souroullas GP. Non-canonical functions of EZH2 in cancer. *Front Oncol.* 2023;13:1233953.
- Wang C, Chen X, Liu X, Lu D, Li S, Qu L, et al. Discovery of precision targeting EZH2 degraders for triple-negative breast cancer. *Eur J Med Chem.* 2022;238:114462.
- Dale B, Anderson C, Park KS, Kaniskan HU, Ma A, Shen Y, et al. Targeting triple-negative breast cancer by a novel proteolysis targeting chimera degrader of enhancer of zeste homolog 2. *ACS Pharm Transl Sci.* 2022;5:491–507.
- Ma A, Stratikopoulos E, Park KS, Wei J, Martin TC, Yang X, et al. Discovery of a first-in-class EZH2 selective degrader. *Nat Chem Biol.* 2020;16:214–22.
- Fischer M, Grossmann P, Padi M, DeCaprio JA. Integration of TP53, DREAM, MMB-FOXM1 and RB-E2F target gene analyses identifies cell cycle gene regulatory networks. *Nucleic Acids Res.* 2016;44:6070–86.
- Huang L, Zhao S, Frasar JM, Dai Y. An integrated bioinformatics approach identifies elevated cyclin E2 expression and E2F activity as distinct features of tamoxifen resistant breast tumors. *PLoS One.* 2011;6:e22274.
- Tsherniak A, Vazquez F, Montgomery PG, Weir BA, Kryukov G, Cowley GS, et al. Defining a cancer dependency map. *Cell.* 2017;170:564–76.e516.
- Lee ST, Li Z, Wu Z, Au M, Guan P, Karuturi RK, et al. Context-specific regulation of NF-kappaB target gene expression by EZH2 in breast cancers. *Mol Cell (Res Support, Non-U S Gov't).* 2011;43:798–810.
- Yang L, Kumegawa K, Saeki S, Nakadai T, Maruyama R. Identification of lineage-specific epigenetic regulators FOXA1 and GRHL2 through chromatin accessibility profiling in breast cancer cell lines. *Cancer Gene Ther.* 2024;31:736–45.
- Keenan AB, Torre D, Lachmann A, Leong AK, Wojciechowicz ML, Utti V, et al. ChEA3: transcription factor enrichment analysis by orthogonal omics integration. *Nucleic acids Res.* 2019;47:W212–W224.
- Chen X, Muller GA, Quaaas M, Fischer M, Han N, Stutchbury B, et al. The forkhead transcription factor FOXM1 controls cell cycle-dependent gene expression through an atypical chromatin binding mechanism. *Mol Cell Biol.* 2013;33:227–36.
- Green AR, Aleskandarany MA, Agarwal D, Elsheikh S, Nolan CC, Diez-Rodriguez M, et al. MYC functions are specific in biological subtypes of breast cancer and confers resistance to endocrine therapy in luminal tumours. *Br J Cancer.* 2016;114:917–28.
- Jeffreys SA, Becker TM, Khan S, Soon P, Neubauer H, de Souza P, et al. Prognostic and predictive value of CCND1/Cyclin D1 amplification in breast cancer with a focus on postmenopausal patients: a systematic review and meta-analysis. *Front Endocrinol (Lausanne).* 2022;13:895729.
- Yan J, Li B, Lin B, Lee PT, Chung TH, Tan J, et al. EZH2 phosphorylation by JAK3 mediates a switch to noncanonical function in natural killer/T-cell lymphoma. *Blood.* 2016;128:948–58.
- Wan L, Xu K, Wei Y, Zhang J, Han T, Fry C, et al. Phosphorylation of EZH2 by AMPK suppresses PRC2 methyltransferase activity and oncogenic function. *Mol Cell.* 2018;69:279–91 e275.
- Jiao L, Shubbar M, Yang X, Zhang Q, Chen S, Wu Q, et al. A partially disordered region connects gene repression and activation functions of EZH2. *Proc Natl Acad Sci USA.* 2020;117:16992–7002.
- Wang L, Chen C, Song Z, Wang H, Ye M, Wang D, et al. EZH2 depletion potentiates MYC degradation inhibiting neuroblastoma and small cell carcinoma tumor formation. *Nat Commun.* 2022;13:12.
- Yu G, Wang LG, Han Y, He QY. clusterProfiler: an R package for comparing biological themes among gene clusters. *OMICS.* 2012;16:284–7.
- Lu J, Guo Y, Yin J, Chen J, Wang Y, Wang GG, et al. Structure-guided functional suppression of AML-associated DNMT3A hotspot mutations. *Nat Commun.* 2024;15:3111.
- Li J, Galbo PM Jr., Gong W, Storey AJ, Tsai YH, Yu X, et al. ZMYND11-MBTD1 induces leukemogenesis through hijacking NuA4/Tip60 acetyltransferase complex and a PWWP-mediated chromatin association mechanism. *Nat Commun.* 2021;12:1045.
- Zhao S, Lu J, Pan B, Fan H, Byrum SD, Xu C, et al. TNRC18 engages H3K9me3 to mediate silencing of endogenous retrotransposons. *Nature.* 2023;623:633–42.
- Curtis C, Shah SP, Chin SF, Turashvili G, Rueda OM, Dunning MJ, et al. The genomic and transcriptomic architecture of 2,000 breast tumours reveals novel subgroups. *Nature.* 2012;486:346–52.
- Pereira B, Chin SF, Rueda OM, Volland HK, Provenzano E, Bardwell HA, et al. The somatic mutation profiles of 2,433 breast cancers refines their genomic and transcriptomic landscapes. *Nat Commun.* 2016;7:11479.

52. Ding L, Bailey MH, Porta-Pardo E, Thorsson V, Colaprico A, Bertrand D, et al. Perspective on oncogenic processes at the end of the beginning of cancer genomics. *Cell*. 2018;173:305–20 e310.
53. Bonneville R, Krook MA, Kautto EA, Miya J, Wing MR, Chen HZ, et al. Landscape of microsatellite instability across 39 cancer types. *JCO Precis Oncol*. 2017;2017:PO.17.00073.
54. Subramanian A, Tamayo P, Mootha VK, Mukherjee S, Ebert BL, Gillette MA, et al. Gene set enrichment analysis: a knowledge-based approach for interpreting genome-wide expression profiles. *Proc Natl Acad Sci USA*. 2005;102:15545–50.

ACKNOWLEDGEMENTS

We thank all members of Cai, Jin and Wang laboratories for helpful discussions during the development of this manuscript. We thank Dr. Bryan Pan for bioinformatics support, Dr. Philip Spanheimer for sharing reagents, and John Albright for technical contributions. We thank core facilities of University of North Carolina and Duke University for their professional support in tissue culture, high-throughput sequencing and bioinformatics and data storage.

AUTHOR CONTRIBUTIONS

JJ, LC and GGW designed the experiments and secured fundings. JC and XY led the biological and medicinal chemistry aspects of the study, respectively, under the supervision of GGW, LC and JJ. JC led on the manuscript writing and all authors conducted data analysis and interpretation and participated in the preparation of manuscript.

FUNDING

This work was supported in part through the UNC Lineberger Comprehensive Cancer Center Core Support Grant P30-CA016086. This work was also supported in part by R01CA262903 (to LC), R01CA218600 (to JJ and GGW), R01CA268519 (to GGW and JJ), R01CA211336 (to GGW) and R01CA230854 (to JJ) grants from the US National Institutes of Health (NIH).

COMPETING INTERESTS

JJ is listed as a co-inventor on the patent application (WO 2018/081530 A1) filed by Icahn School of Medicine at Mount Sinai covering EZH2 degraders. JJ is a cofounder and equity shareholder in Cullgen, Inc. and a consultant for Cullgen, Inc., EpiCypher, Inc., and Accent Therapeutics, Inc. The Jin laboratory received research funds from Celgene Corporation, Levo Therapeutics, Inc., Cullgen, Inc., and Cullinan Oncology, Inc.

ETHICS DECLARATIONS

This study does not require ethics approval because no animals and human subjects are used.

ADDITIONAL INFORMATION

Supplementary information The online version contains supplementary material available at <https://doi.org/10.1038/s41388-024-03119-9>.

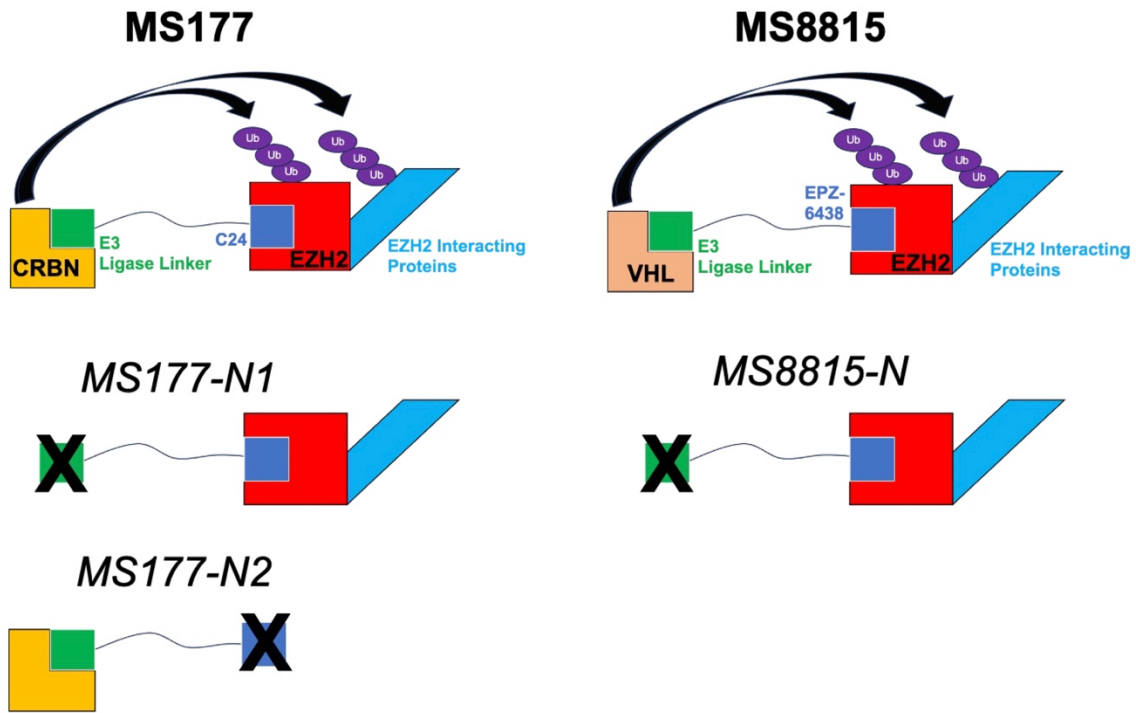
Correspondence and requests for materials should be addressed to Ling Cai or Gang Greg Wang.

Reprints and permission information is available at <http://www.nature.com/reprints>

Publisher's note Springer Nature remains neutral with regard to jurisdictional claims in published maps and institutional affiliations.

Springer Nature or its licensor (e.g. a society or other partner) holds exclusive rights to this article under a publishing agreement with the author(s) or other rightsholder(s); author self-archiving of the accepted manuscript version of this article is solely governed by the terms of such publishing agreement and applicable law.

A



B

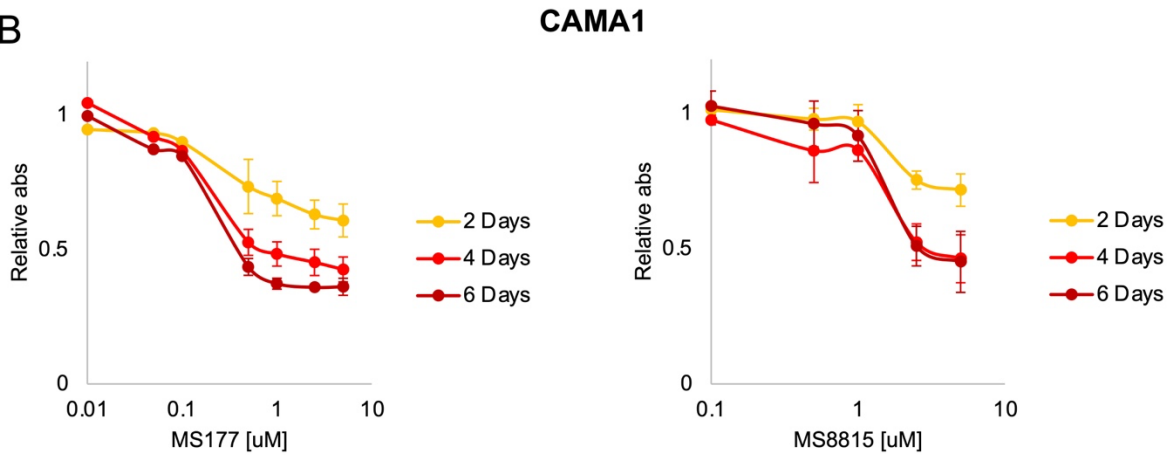
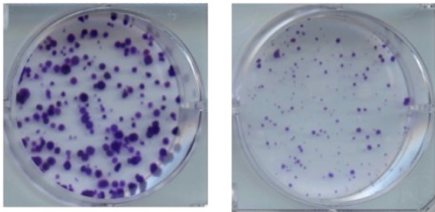


Figure S1: Models of EZH2 targeted PROTACs MS177 and MS8815, and both PROTACs decrease growth of CAMA1 cells.

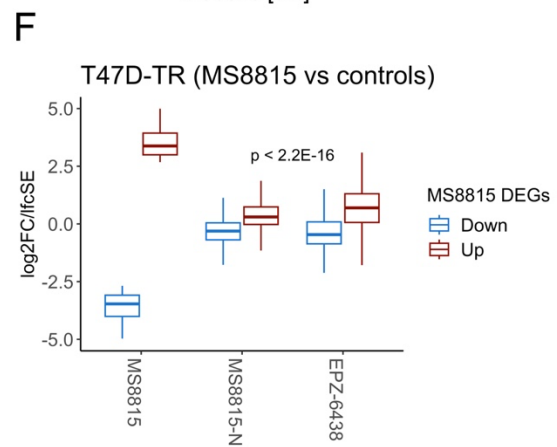
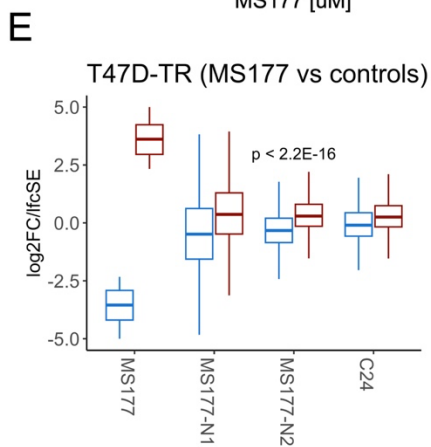
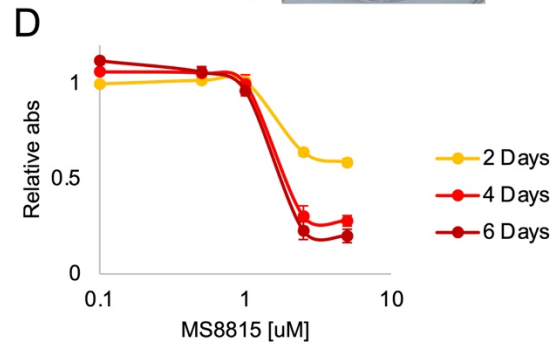
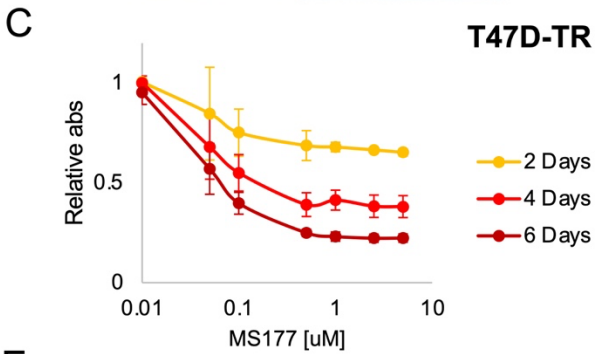
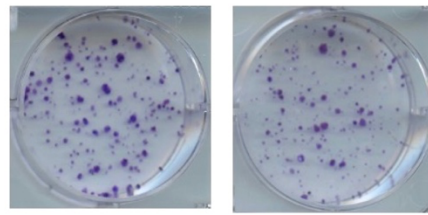
A) Models of MS177 (Left) and MS8815 (Right) and respective negative controls. MS177 contains the C24 EZH2 methyltransferase inhibitor tethered to the CRBN E3 ligase via a linker. Negative controls: MS177-N1 contains a modified, CRBN E3 ligase-binding-defective moiety, and MS177-N2 contains a modified C24 moiety with a compromised activity in EZH2 methyltransferase inhibition. MS8815 contains the EPZ-6438 EZH2 methyltransferase inhibitor tethered to the VHL E3 ligase via a linker. Negative control: MS8815-N contains a modified, VHL E3 ligase-binding-defective moiety.

B) Plots showing relative absorbances from MTS assays of CAMA1 cells treated with labelled concentrations of MS177 (Left) or MS8815 (Right) for 2, 4 or 6 days. Relative absorbance numbers presented were calculated relative to cells grown treated with DMSO vehicle control. N = 3 biological replicates. Error bars represent mean \pm s.d.

A **T47D**
EtOH 1 uM Tamoxifen



B **T47D-TR**
EtOH 1 uM Tamoxifen



G MS117/MS8815 DEGs DepMap CRISPR Effect

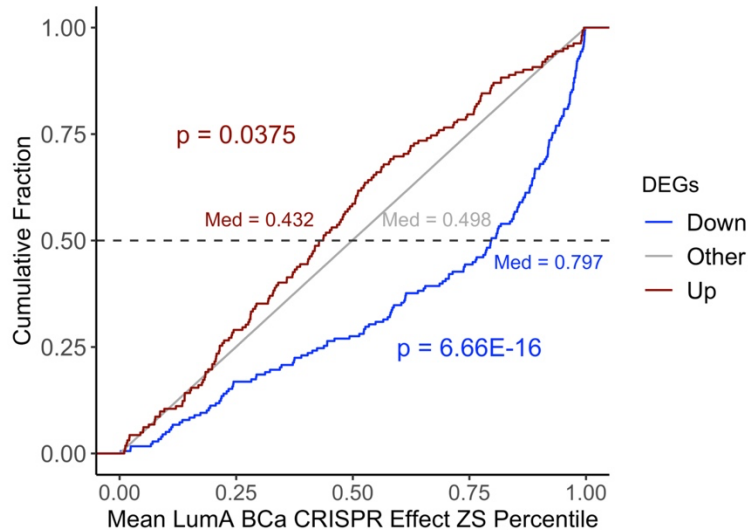


Figure S2: MS177 and MS8815 inhibit tamoxifen-resistant BCa cell growth and reduce the expression of essential genes.

A,B) Colony formation assays of T47D (**A**) and T47D-TR (**B**) cell lines grown in the presence of 1 μ M tamoxifen or ethanol (EtOH) vehicle control.

C,D) Plots showing relative absorbances from MTS assays of T47D-TR cells treated with labelled concentrations of MS177 (**C**) or MS8815 (**D**) for 2, 4 or 6 days. Relative absorbance numbers presented were calculated relative to cells grown treated with DMSO vehicle control. N = 3 biological replicates. Error bars represent mean \pm s.d.

E,F) Box plots showing the log₂ fold change divided by standard error (log₂FC/lfcSE) values of genes significantly downregulated (blue) and upregulated (red) by MS177 (**G**) and MS8815 (**H**) determined by RNAseq of RNA extracted from T47D-TR cells treated with 2.5 μ M MS177, MS177-N1, MS177-N2, C24 or 2.5 μ M MS8815, MS8815-N, EPZ-6438 for 48 hours or 30 hours – respectively - compared to DMSO vehicle control. P-values were calculated comparing all other respective treatments to MS177 or MS8815 for downregulated and upregulated genes separately using two-sided t-test. P-values were adjusted using Bonferroni's method, and $p < 2.2E-16$ applies to all comparisons.

G) Plot showing the cumulative distribution of genes significantly downregulated (184 genes, blue) and upregulated (174 genes, red) by MS177 in T47D and T47D-TR cells and MS8815 in T47D-TR cells (see figure 3E) - compared to all other genes (17113 genes, grey) - among all genes ranked ordered by percentile of mean z-score normalized CRISPR effect scores obtained from the DepMap database. High percentile indicates more essential and low percentile indicates less essential. P-values were calculated by KS test, and median percentiles are labelled by group.

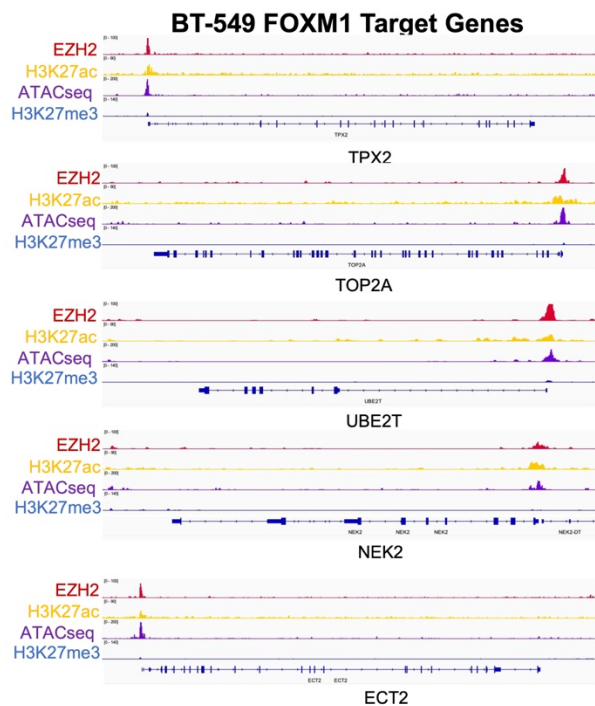
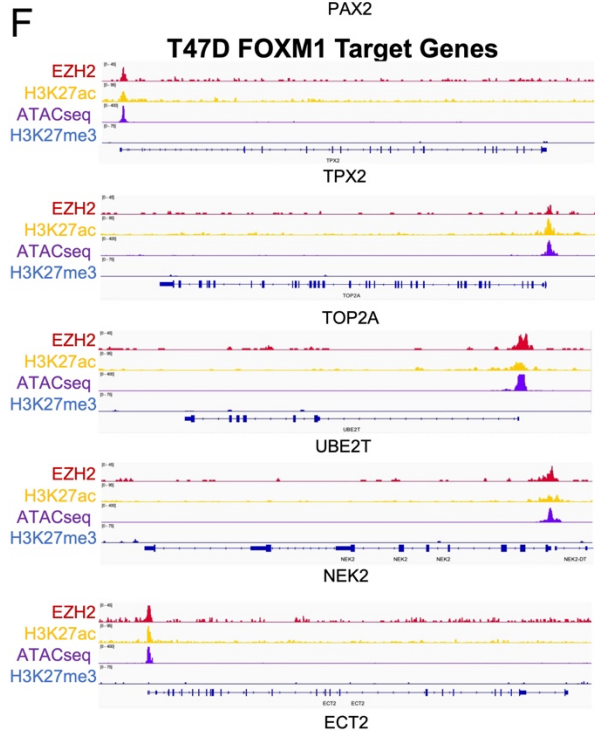
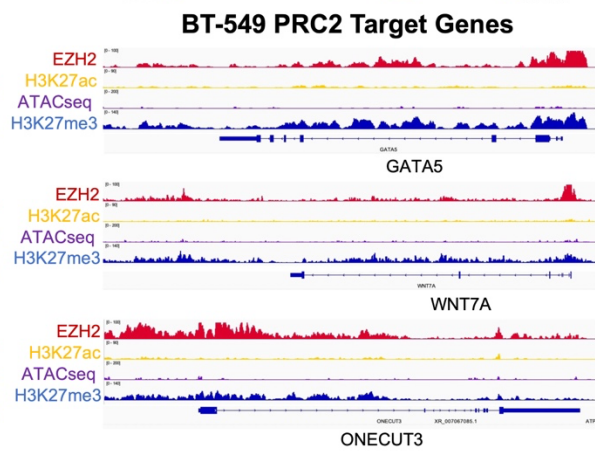
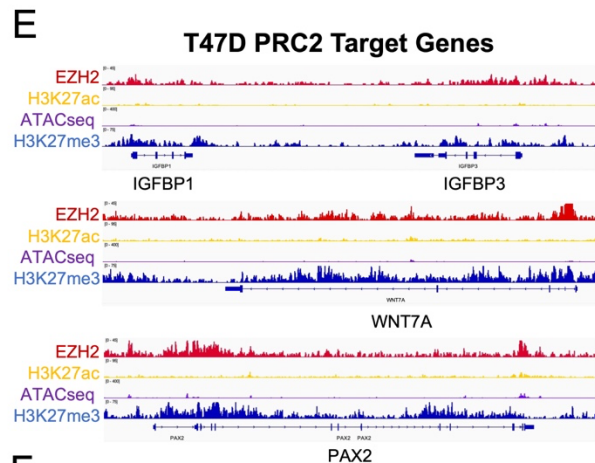
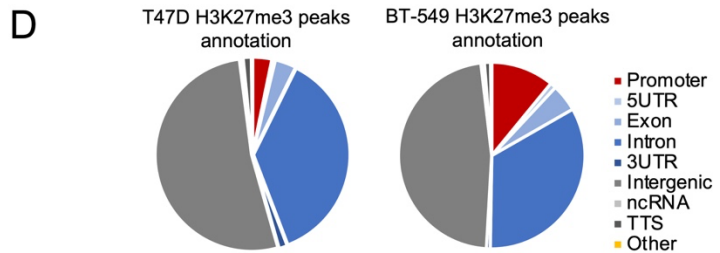
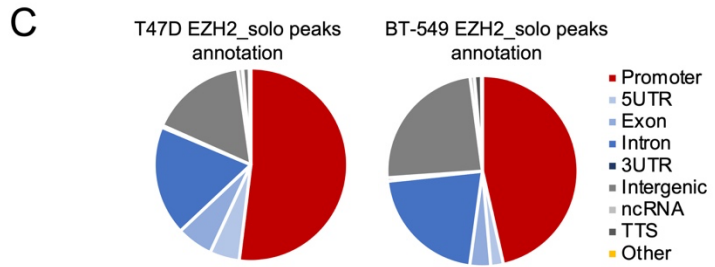
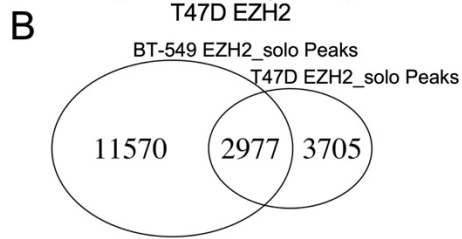
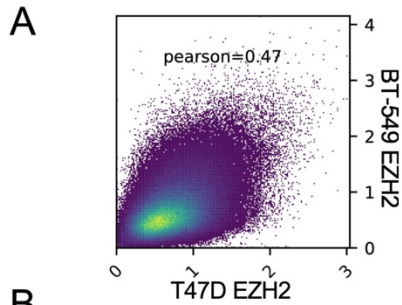


Figure S3: EZH2 binds to the promoter regions of FOXM1 target genes lacking the H3K27me3 repressive mark in T47D and BT-549 cell lines.

A) Scatter plot showing the correlation of EZH2 CUT&RUN read distribution in T47D and BT-549 cells.

B) Venn diagram showing the overlap of EZH2_solo peaks in T47D and BT-549 cells.

C-D) Pie charts showing categories for EZH2_solo peak (C) and H3K27me3 peak (D) annotations for T47D (Left) and BT-549 (Right) cells.

E-F) IGV tracks showing the CUT&RUN and CUT&Tag read densities for EZH2, H3K27ac and H3K27me3, as well as ATAC-seq[35], at select PRC2 target genes (genes associated with H3K27me3 peaks) (E) and FOXM1 target genes (TPX2, TOP2A, UBE2T, NEK2, ECT2) (F) in T47D (Left) and BT-549 (Right) cell lines.

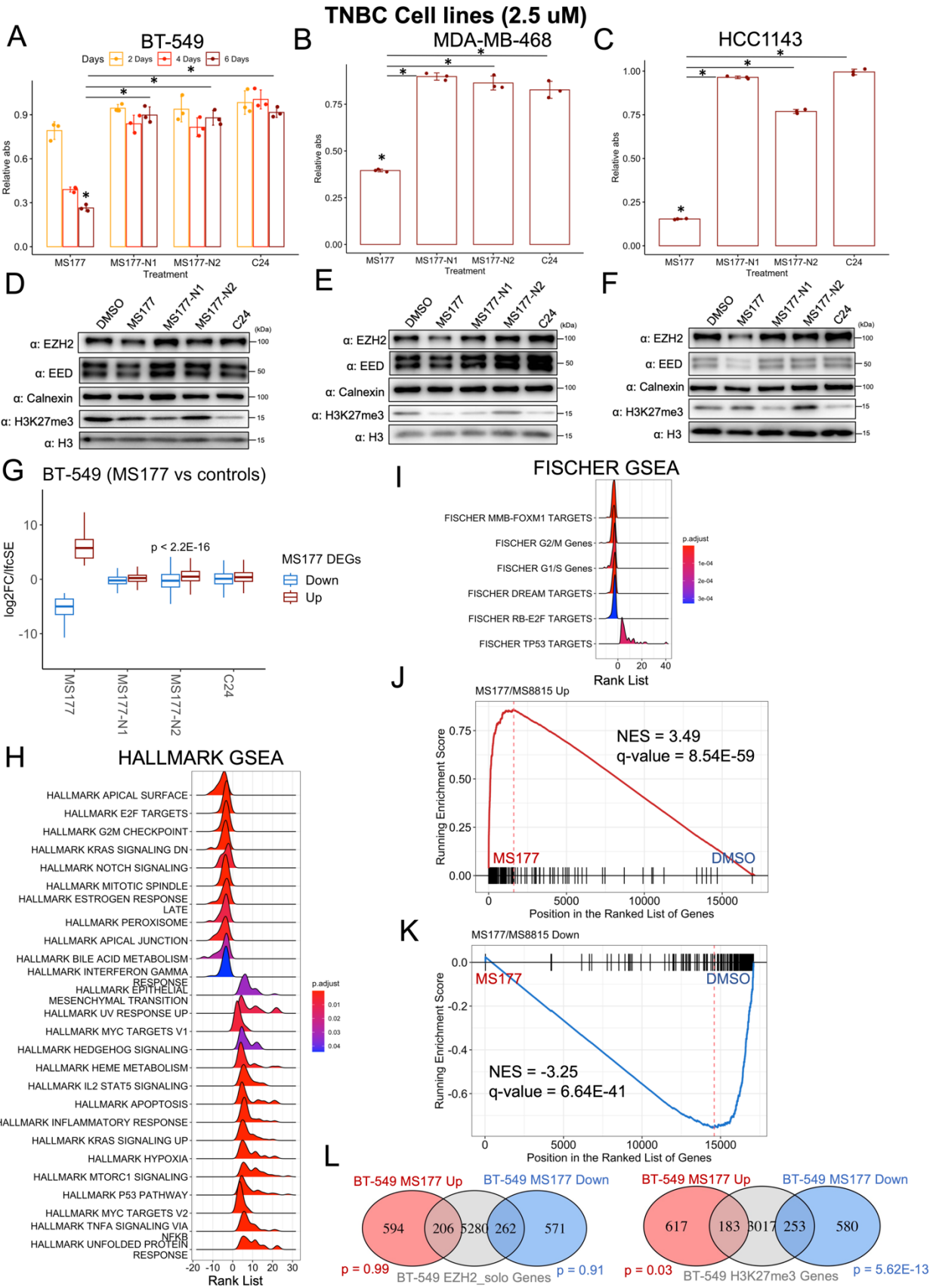


Figure S4: EZH2 targeted PROTACs reduce triple negative breast cancer cell growth and reduce the expression of cell cycle related gene sets.

A-C) Bar graphs showing relative absorbances from MTS assays of BT-549 cells treated with 2.5 μ M MS177, MS177-N1, MS177-N2 or C24 for 2, 4 or 6 days (**A**), as well as MDA-MB-468 (**B**) and HCC1143 (**C**) cells treated with the same compounds for 6 days. Relative absorbance numbers presented were calculated relative to cells grown treated with DMSO vehicle control. N = 3 biological replicates, p-values calculated by two-sided t-test and adjusted using Bonferroni's method; * p < 0.05. Error bars represent mean \pm s.d.

D-F) Western blots showing EZH2 and H3K27me3 protein expression in lysates from BT-549 (**D**), MDA-MB-468 (**E**) and HCC1143 (**F**) cell lines treated with 2.5 μ M MS177, MS177-N1, MS177-N2, C24 or DMSO vehicle control. Cells were treated with labelled compounds for 48 hours prior to cell lysis and subsequent western blot analyses. Calnexin and H3 were used as loading controls for whole cell protein and histones, respectively.

G) Box plot showing the log₂ fold change divided by standard error (log₂FC/lfcSE) values of genes significantly downregulated (blue) and upregulated (red) by MS177 determined by RNA-seq of RNA extracted from BT-549 cells treated with 2.5 μ M MS177, MS177-N1, MS177-N2, C24 for 48 hours compared to DMSO vehicle control. P-values were calculated comparing MS177-N1, MS177-N2 and C24 to MS177 for downregulated and upregulated genes separately using two-sided t-test. P-values were adjusted using Bonferroni's method, and p < 2.2E-16 applies to all comparisons.

H-K) Ridge plots showing HALLMARK geneset (**H**), Fischer cell cycle geneset[31] (**I**), with significant negative and positive associations - and enrichment plots showing gene sets of genes downregulated (184 genes) (**J**) and upregulated (174 genes) (**K**) by EZH2 PROTAC treatment in T47D and T47D-TR cells (see figure 3E) - with MS177 treatment of BT-549 cells compared to DMSO control, as determined by GSEAs from RNA-seq. P-values were adjusted using FDR, and adjusted q-values < 0.05 were considered significant.

L) Venn diagrams showing the overlap of EZH2 solo genes (Left) and H3K27me3 associated genes (Right) in BT-549 cells and genes upregulated (red) and downregulated (blue) by MS177 in BT-549 cells as determined by RNA-seq. P-values calculated by hypergeometric distribution are labelled next to each pairwise overlap.

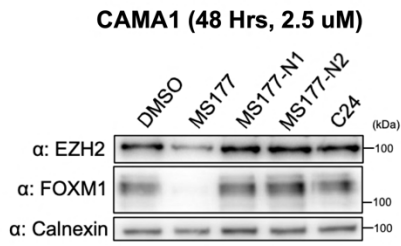
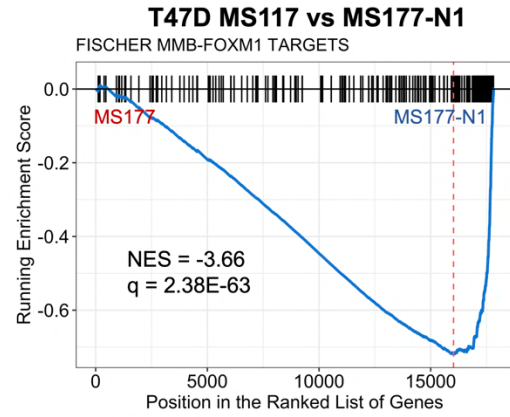
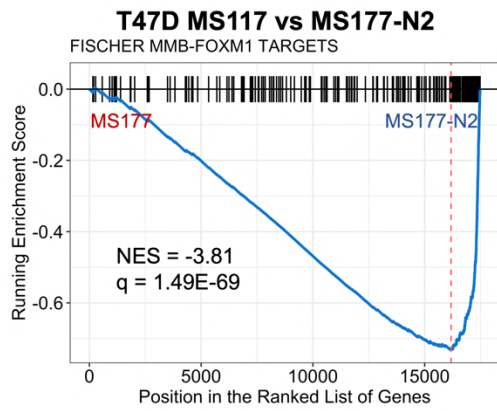
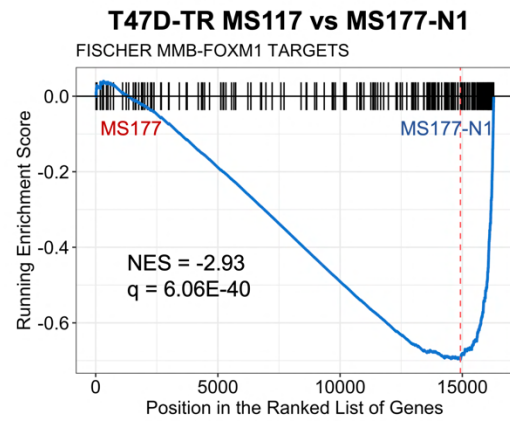
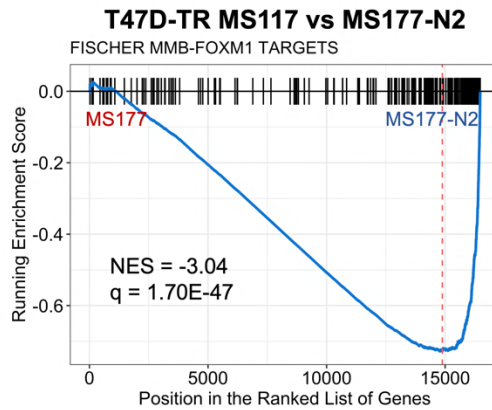
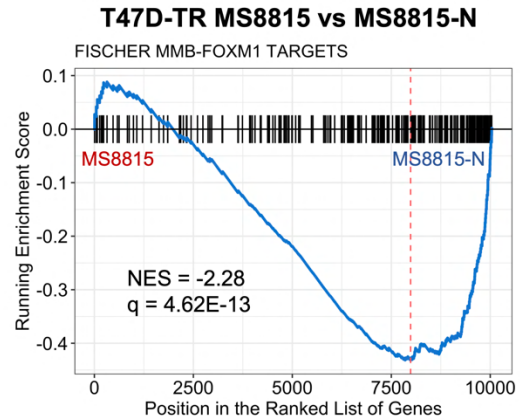
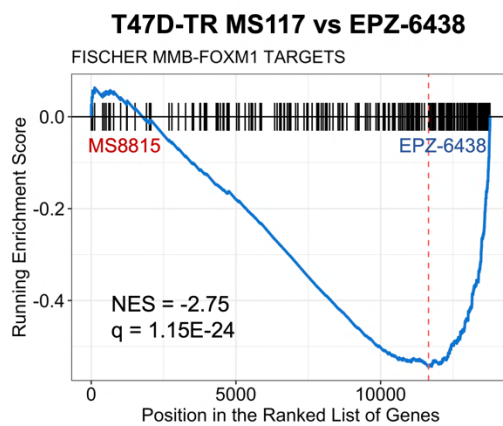
A**B****C****D****E****F****G**

Figure S5: EZH2 targeted PROTACs significantly reduce FOXM1 protein and FOXM1 target gene expression compared to EZH2 methyltransferase inhibitors or negative controls.

A) Western blots showing EZH2 and FOXM1 protein expression in lysates from CAMA1 cells treated with 2.5 μ M MS177, MS177-N1, MS177-N2, C24 or DMSO vehicle control. Cells were treated with labelled compounds for 48 hours prior to cell lysis and subsequent western blot analyses. Calnexin was used as loading control.

B-C) Enrichment plots showing Fischer MMB-FOXM1 target geneset[31] enrichment in T47D cells treated with MS177 compared to MS177-N1 (**B**) or MS177-N2 (**C**), as determined by GSEAs from RNA-seq results. P-values were adjusted using FDR, and q-values < 0.05 were considered significant.

D-G) Enrichment plots showing Fischer MMB-FOXM1 target geneset[31] enrichment in T47D-TR cells treated with MS177 compared to MS177-N1 (**D**) or MS177-N2 (**E**), or treated with MS8815 compared to MS8815-N (**F**) or EPZ-6438 (**G**), as determined by GSEAs from RNA-seq results. P-values were adjusted using FDR, and q-values < 0.05 were considered significant.

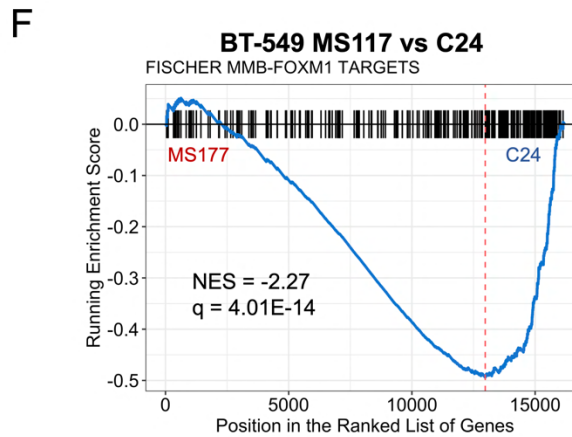
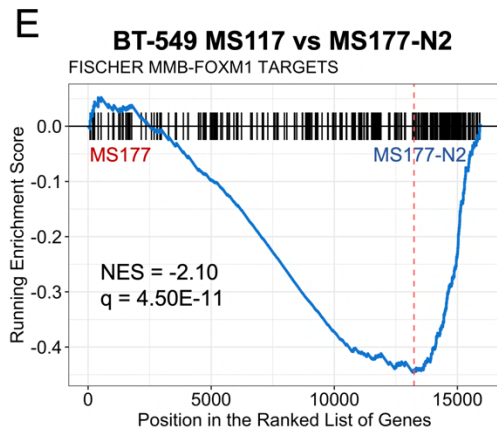
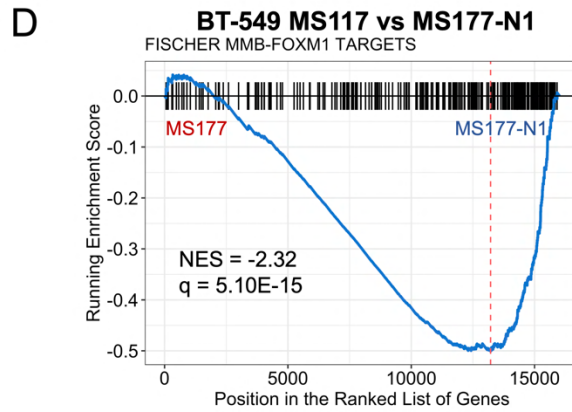
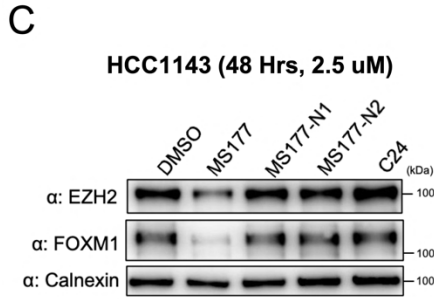
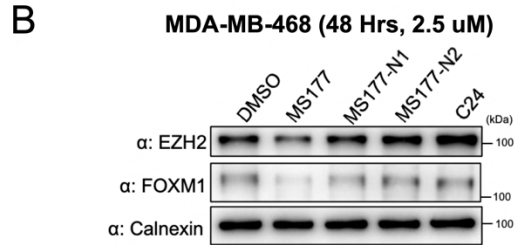
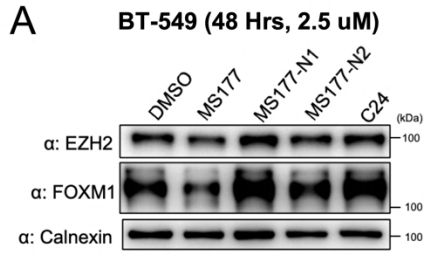


Figure S6: EZH2 targeted PROTACs reduce FOXM1 protein expression in triple negative breast cancer cell lines.

A-C) Western blots showing EZH2 and FOXM1 protein expression in lysates from BT-549 (**A**), MDA-MB-468 (**B**) and HCC1143 (**C**) cell lines treated with 2.5 uM MS177, MS177-N1, MS177-N2, C24 or DMSO vehicle control. Cells were treated with said compounds for 48 hours prior to cell lysis and subsequent western blot analyses. Calnexin was used as loading control.

D-F) Enrichment plots showing Fischer MMB-FOXM1 target geneset [31] enrichment in BT-549 cells treated with MS177 compared to MS177-N1 (**D**), MS177-N2 (**E**) or C24 (**F**), as determined by GSEAs from RNA-seq results. P-values were adjusted using FDR, and q-values < 0.05 were considered significant.

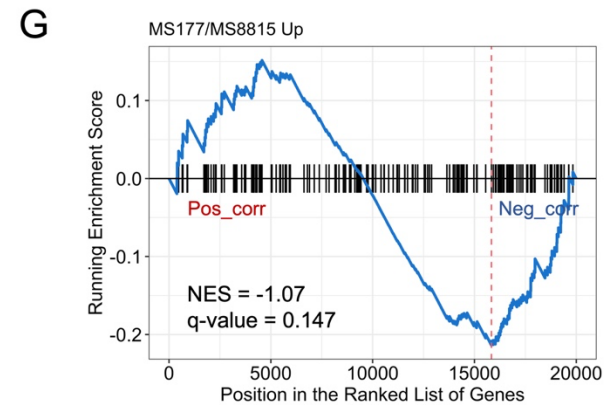
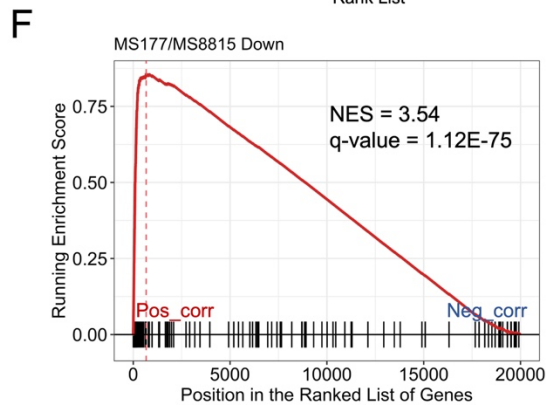
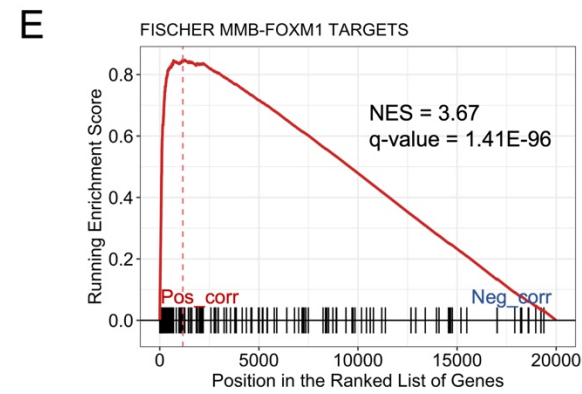
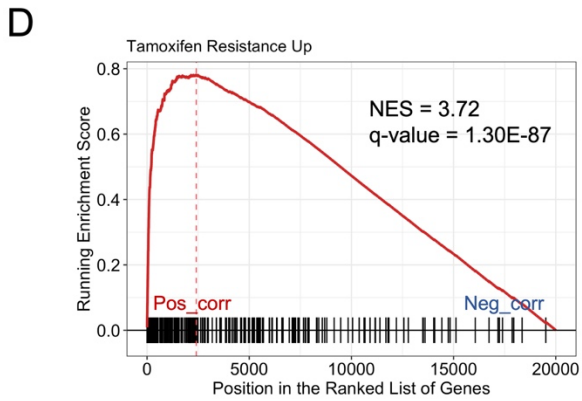
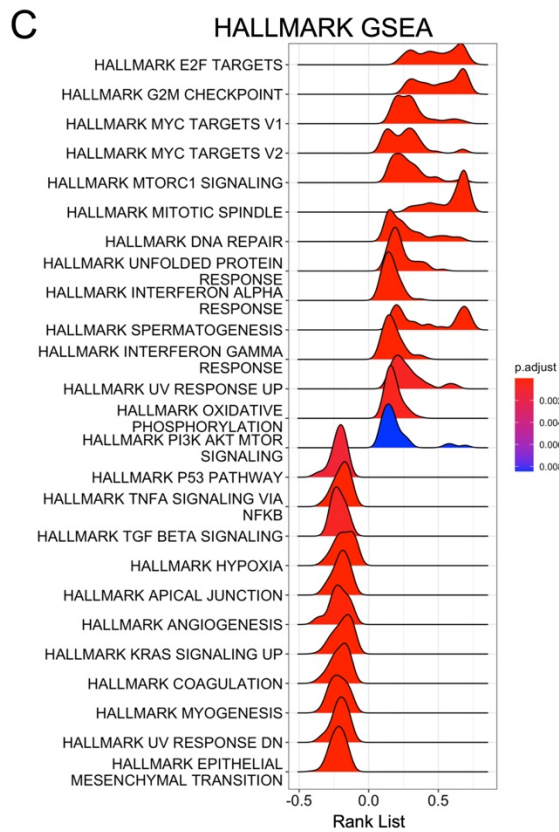
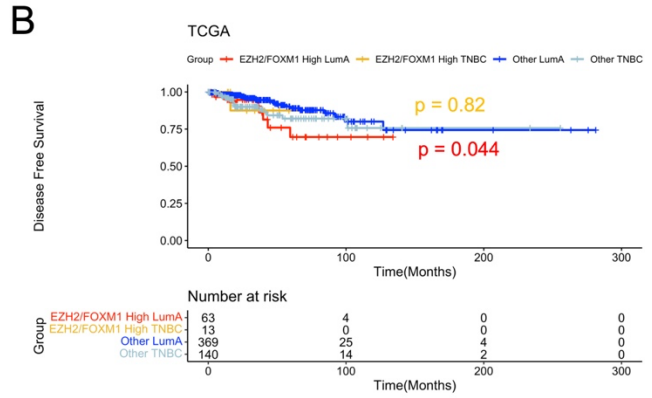
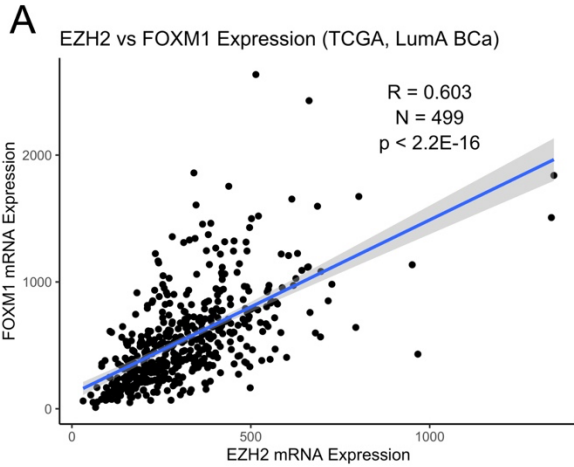


Figure S7: EZH2 mRNA expression correlates with FOXM1, FOXM1 target genes, cell cycle regulated gene sets, and genes associated with tamoxifen resistance in luminal A breast cancer clinical samples from the TCGA study.

A) Scatter plot showing correlation between EZH2 and FOXM1 mRNA expression from luminal A breast cancer samples from the TCGA study[48, 49] (N=499).

B) Kaplan-Meier plot showing the relapse free survival of luminal A BCa and TNBC patients from the METABRIC study stratified by EZH2 and FOXM1 high mRNA expression (higher than 75th percentile for both genes, LumA N=63, TNBC N=13) and all other patient samples for each subtype (LumA N=369, TNBC N=140). P-values for each subtype were calculated by log-rank test.

C) Ridge plots showing HALLMARK gene sets with significant negative and positive associations – as determined by GSEA - with genes rank ordered by Spearman correlation r-values with EZH2 mRNA expression within luminal A breast cancer samples from the TCGA study.

D-G) Enrichment plots from GSEAs using gene sets comprised of genes associated with tamoxifen resistance [32] **(D)** FOXM1 target genes [31] **(E)** and genes downregulated **(F)** and upregulated **(G)** by EZH2 PROTAC treatment in T47D and T47D-TR cells, as determined by RNA-seq (see figure 3E). Genes were rank ordered as stated above in 6C. P-values were adjusted by FDR (q-value) and $q < 0.05$ was considered significant.

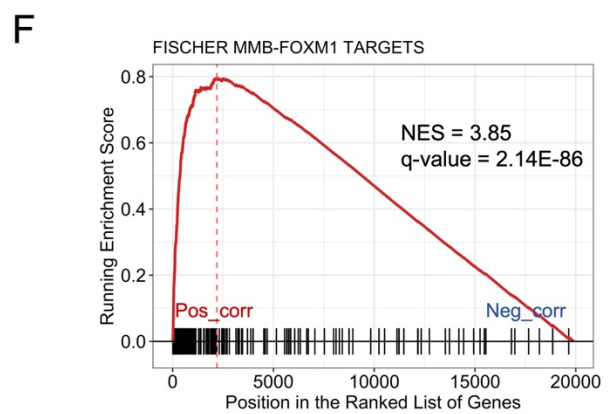
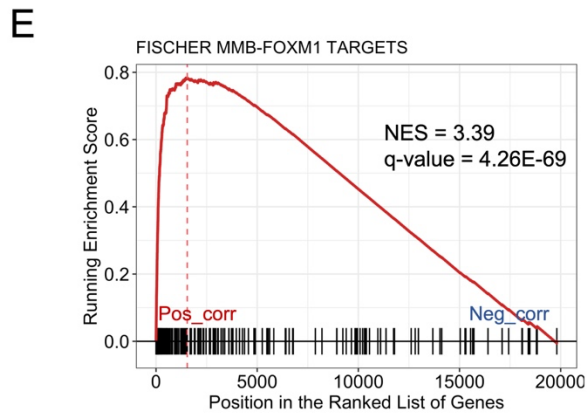
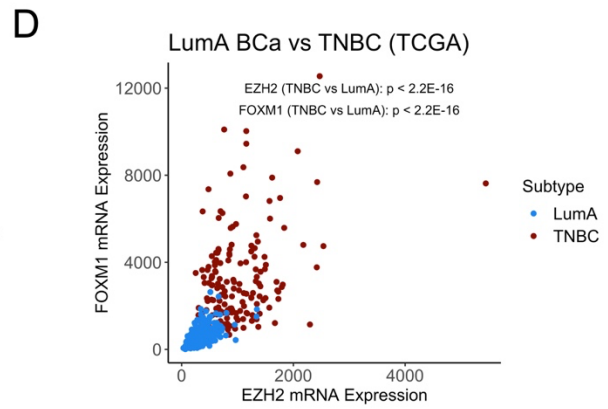
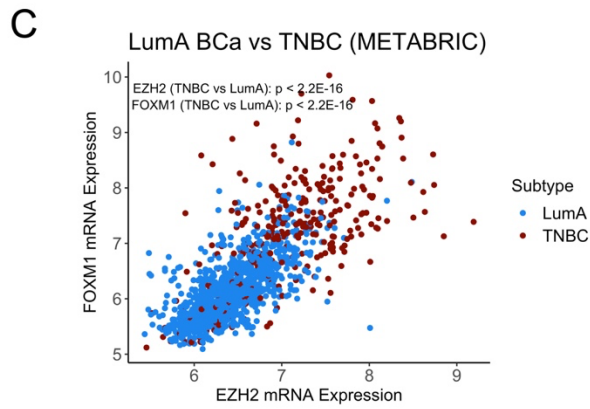
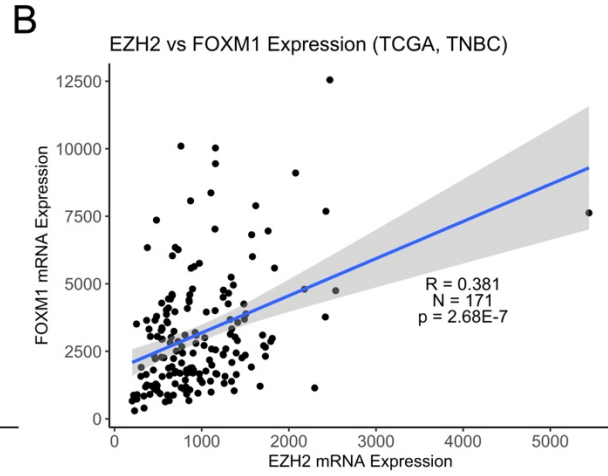
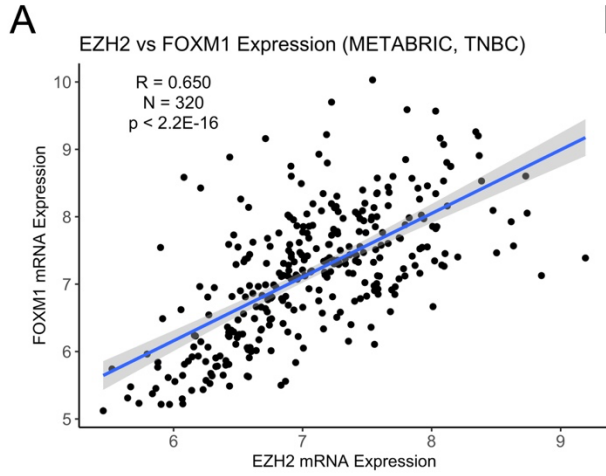


Figure S8: EZH2 mRNA expression correlates with FOXM1 and FOXM1 target genes in triple negative breast cancer clinical samples from METABRIC and TCGA studies.

A-B) Scatter plot showing correlation between EZH2 and FOXM1 mRNA expression from triple negative breast cancer (TNBC) samples from the METABRIC [46, 47] (N = 320) **(A)** and TCGA [48, 49] (N = 171) **(B)** studies.

C-D) Scatter plot showing EZH2 and FOXM1 mRNA expression from LumA BCa (Blue) and TNBC (Red) samples from the METABRIC **(C)** and TCGA **(D)** studies. Significance was determined for differential FOXM1 and EZH2 expression between LumA BCa and TNBC. P-values were calculated by KS test from TNBC and LumA samples rank ordered by EZH2 and FOXM1 mRNA expression independently.

E-F) Enrichment plots of Fischer MMB-FOXM1 targets gene set [31] – as determined by GSEA - with genes rank ordered by Spearman correlation r-values with EZH2 mRNA expression within triple negative breast cancer samples from the METABRIC **(E)** and TCGA **(F)** studies. P-values were adjusted by FDR (q-value) and $q < 0.05$ was considered significant.